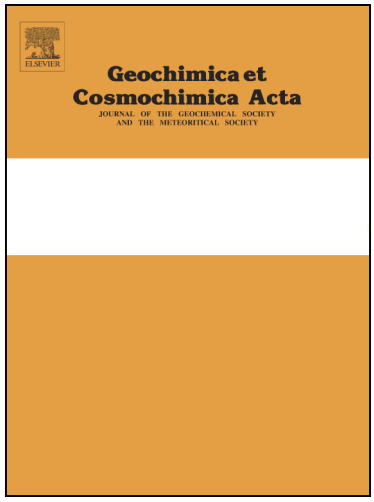

Chemical and mineralogical characterisation of illite–smectite: Implications for episodic tectonism and associated fluid flow, central australia

Alexander W. Middleton, I. Tonguç Uysal, Suzanne D. Golding

PII: S0016-7037(14)00593-6
DOI: http://dx.doi.org/10.1016/j.gca.2014.09.035
Reference: GCA 8998

To appear in: *Geochimica et Cosmochimica Acta*

Received Date: 14 March 2014
Accepted Date: 25 September 2014

Please cite this article as: Middleton, A.W., Tonguç Uysal, I., Golding, S.D., Chemical and mineralogical characterisation of illite–smectite: Implications for episodic tectonism and associated fluid flow, central australia, *Geochimica et Cosmochimica Acta* (2014), doi: http://dx.doi.org/10.1016/j.gca.2014.09.035

CHEMICAL AND MINERALOGICAL CHARACTERISATION OF ILLITE–SMECTITE: IMPLICATIONS FOR EPISODIC TECTONISM AND ASSOCIATED FLUID FLOW, CENTRAL AUSTRALIA

Alexander W. Middleton*[ab], I. Tonguç Uysal[a] and Suzanne D. Golding[b]

[a] *Queensland Geothermal Energy Centre of Excellence, The University of Queensland, Queensland 4072, Australia*

[b] *School of Earth Science, The University of Queensland, Queensland 4072, Australia*

Abstract

The Warburton–Cooper–Eromanga basins of central–eastern Australia contain a number of reactivated fracture–fault networks that relate to a complex and poorly understood thermal and tectonic evolution. Authigenic illite was sampled from two prominent features of the Warburton–Cooper basins: the Gidgealpa–Merrimelia–Innamicka Ridge, composed of anticlinal imbricate thrust fault blocks, and the synclinal Nappamerri Trough. These sample sets were investigated using a combination of clay mineralogical, trace element and stable isotope analyses to deduce the palaeofluid chemistry associated with past tectonothermal perturbations. The Nappamerri Trough hosts the highly radiogenic Big Lake Suite granite and part of Australia's largest on-shore oil and gas reserves. Calculated fluid stable isotope values from the trough, in conjunction with calculated palaeotemperatures, indicate an influx of evolved high-latitudinal meteoric waters under an extremely high geothermal gradient (~100 °Ckm^{-1}) and high water/rock ratios consistent with an extensional environment. Such high water/rock ratios resulted in intense alteration of the granite during which it underwent substantial enrichment in the heat-producing elements (HPE),

particularly Th. This hydrothermal system is interpreted to result from continent-wide transmission of tensional stress originating from episodic rifting of the eastern Australian margin in the mid Cretaceous, as dated by Sm–Nd, Rb–Sr and Ar–Ar. The Gidgealpa–Merrimelia–Innamincka Ridge, by contrast, is marked by a lower, but still elevated, palaeogeothermal gradient (~42 °Ckm^{-1}) and calculated fluid isotopic values compatible with evolved basinal fluids of meteoric origin under low water/rock ratio conditions. Distinct trace element compositions of residue and leachate aliquots further indicate two periods of fluid flow with unique chemical compositions. In light of previous geochronology, these events are interpreted as westward extensions of widespread crustal tensional stress that affected much of central and eastern Queensland in the Carboniferous and Late Triassic

Integrated analyses of authigenic illite provide evidence for three periods of fluid flow and elevated thermal regime associated with regional tectonism during the Carboniferous, Late Triassic and Cretaceous. Our data further show that due to the extremely high geothermal gradient and water/rock ratios, Cretaceous fluid flow had profound effects on the surrounding geology, which may have formed/enhanced two of Australia's most significant energy resources.

Corresponding author Tel: +61 422708045

Email Address: alexander.middleton@uqconnect.edu.au

Keywords: Thermal and tectonic history, Warburton–Cooper–Eromanga basins, stable isotopes, trace elements, illite.

1. INTRODUCTION

Rapid adjustments to intra-continental stress fields can perturb the thermal and fluid flow regimes of sedimentary basins, leading to the expulsion of basinal fluids (Kyser, 2007). During the migration of tectonically-driven fluids along permeable fracture networks, fluid–rock interaction results in the precipitation of authigenic phases, including illite. Due to its composition, illite can be used for a number of geochronological and geochemical techniques (Clauer et al., 1993; Zwingmann et al., 1999; Uysal et al., 2000c; Uysal et al., 2006; Verdel et al., 2012; Middleton et al., 2014). High magnification microscopy of illite may reveal paragenetic and morphological data pertinent to constraining fluid–rock interaction history (Reuter and Dallmeyer, 1987; Yau et al., 1987; Wilson et al., 2014). Stable isotopic analysis of authigenic clays can also determine fluid source, and by understanding typical variations in isotopic values, can constrain fluid evolution (Longstaffe, 2000). Trace element studies of authigenic clays have similarly proven useful in determining physico-chemical conditions during fluid–rock interaction (Bau, 1991; Bau and Dulski, 1995; Zwingmann et al., 1999; Bau et al., 2003; Uysal and Golding, 2003).

The Warburton–Cooper–Eromanga basins host one of Australia's largest on-shore petroleum reserves. Previous work by Deighton and Hill (1998) constrained maturation and expulsion of such reserves to the "mid Cretaceous"; however, the thermal regime responsible for such expulsion is not well constrained. These basins also host one of the most prospective hot dry-rock geothermal resources in world, which may stem from the presence of the highly radiogenic Big Lake Suite A-type granite (up to 144 ppm Th and 30 ppm U; Marshall, 2014). Early workers believed zircons to be the primary sink for heat-producing elements (HPE; K, Th and U) in the Big Lake Suite. Chemical and microscopic analyses have since shown some highly enriched areas to be deficient of zircons, due to intense

hydrothermal alteration (Middleton, 2014). As such, the source and origin of the granite's radiogenic nature is still unknown. Previous tectono-stratigraphic studies identified widespread reactivated fault–fracture networks pointing towards a complex, and poorly understood tectonic and thermal evolution that leaves >180 Ma of unrecorded basinal history (Apak et al., 1997; Sun, 1999; Mavromatidis, 2008). Such fracture networks would have acted as highly permeable conduits for hydrothermal fluid flow during past tectonothermal activity, which would have resulted in the precipitation of authigenic clays. Therefore, geochemical analysis of these authigenic phases may shed light on the tectonic and thermal history of these basins as well as the formation of two of Australia's more prominent energy resources.

A complementary high-resolution geochronological study by Middleton et al. (2014) identified three periods of significant fluid flow that differentially affected regions of the Warburton–Cooper basins. These data show that, while episodic Cretaceous (128–86 Ma) fluid flow events were restricted to the Nappamerri Trough, Carboniferous (323.3 ± 9.4 Ma) and Jurassic (201.7 ± 9.3 Ma) events were basin-wide and hence, are still recorded in the structurally high Gidgealpa–Merrimelia–Innamincka Ridge. In this paper we interpret a combination of trace element, stable isotope and clay mineralogical data and aim to constrain the physico-chemical conditions during tectonically-derived fluid flow. By building on previous geochronological (Middleton et al., 2014) and structural data (Apak et al., 1995; Apak et al., 1997; Sun, 1997; Mavromatidis, 2008), this work attempts to reconstruct the thermal and fluid flow history of one of the world's more enigmatic sedimentary basins.

2. GEOLOGICAL SETTING

The stacked Warburton–Cooper–Eromanga basins extend from south-east Queensland ca. 700 km into north-west South Australia (Fig. 1a) and comprise the early Palaeozoic Warburton Basin, unconformably overlain by the Permian-Carboniferous Cooper and Late Triassic-Cretaceous Eromanga basins. The Warburton Basin is interpreted to have formed in a back-arc basin setting to the west of the Mt. Wright arc, implying the presence of westward subduction (Roberts et al., 1990). The Cambrian, bimodal Mooracoochie Volcanics, including the "Jena basalt", form the base of the Warburton Basin and are unconformably overlain by mid-upper Cambrian shales and carbonates and Ordovician siltstones and shales (Gatehouse, 1986; Meixner et al., 1999). The Warburton Basin succession is intruded by the Big Lake Suite (BLS) A-type granite (Marshall, 2014) that has been attributed to the Alice Springs Orogeny (Sun, 1997) and dated at 298 ± 4 and 323 ± 5 Ma (preferred SHRIMP ages) from the western (Moomba 1) and eastern (McLeod 1) cupolas, respectively (Gatehouse et al., 1995). The BLS has two predominant cupolas that comprise the "Moomba High" and are bounded by normal faults (Apak et al., 1995).These cupolas (Fig. 1b) are unusually enriched in HPE: K, Th and U. The origin of enrichment is currently unknown, but has lead to substantial research and attempts to utilise the BLS for an enhanced geothermal system (Chopra and Wyborn, 2003). Enhanced geothermal systems work by injection of cool water down an injection well where it is heated by the fractured, surrounding country-rock. Heated water then flows, under pressure, up production wells where heat is extracted for the production of electricity, as seen at the Soultz-sous-Forêts geothermal project, France (Gerard, 2006).

Unconformably overlying the Warburton Basin and BLS granite are the Cooper and Eromanga basins that are arguably considered to be intra-continental, sag basins (Apak et al., 1997; Cook et al., 2013). Prior to the onset of deposition of Cooper Basin sediments, the BLS experienced uplift and erosion, shedding U and Th-enriched sediment

that would later comprise the "Tirrawarra conglomerate" (Meixner et al., 1999). The Cooper Basin developed structurally by the reactivation of previous faults until a period of tectonic quiescence. During this time, the Gidgealpa (late Carboniferous–late Permian) and Nappamerri (late Permian–late Triassic) Groups were deposited (Alexander, 1998). These groups are further subdivided into the coal-bearing Tirrawarra, Patchawarra, 'Moomba' and Toolachee Formations, and the Arrabury and Tinchoo Formations, respectively. Sediments include a complicated mix of sandstones, siltstones, diamictites, conglomeratic mudstones and shale (Alexander, 1998). The Gidgealpa–Merrimelia–Innamincka (GMI) Ridge is the most prominent NE–SW trending anticlinal thrust structure that is interpreted as Late Carboniferous, and divides the Patchawarra and Nappamerri synclinal troughs of the Cooper Basin (Sun, 1997; and references therein). Sediment thickness in the Patchawarra Trough is less than half that seen in the Nappamerri Trough, due to its topographic height (Gravestock and Jensen-Schmidt, 1998). Sedimentation then ceased due to apparent northeast-southwest compression, resulting in basin-wide exhumation and formation of the Nappamerri Unconformity (Thornton, 1979; Kuang, 1985). Subsequent subsidence and sedimentation of the Eromanga Basin deposited near uniform, Late Triassic to Cretaceous fluvial-lacustrine and shallow marine sediments until exhumation at the Upper Cretaceous–Palaeogene boundary. The following 90 Myr are characterised by minimal sedimentation and multiple periods of exhumation (Mavromatidis, 2006; Mavromatidis, 2008).

3. SAMPLING AND ANALYTICAL PROCEDURES

3.1. Sampling

Granitic and sedimentary rock samples were collected from multiple drill holes along the GMI Ridge and within the Nappamerri Trough (Fig. 1). Twelve samples were taken from Warburton Basin sediments along the GMI Ridge (Gidgealpa 1, Merrimelia 1 – 3, Tirrawarra 1, 7 and 10 and Wantana 1). A further 21 samples were taken from Warburton and Cooper basin sediments and the BLS granite of the Nappamerri Trough (Moomba 1, 2, 7 and 72, Big Lake 1 and 57 and McLeod 1). As samples were collected from both Warburton and Cooper Basin stratigraphy, they will be collectively referred to as Nappamerri Tough or GMI Ridge samples throughout the paper. If referring to samples from an entire drill hole., the drill hole name will be given with no specific depth, for example Moomba 72. If a specific sample and depth is referred to then the full sample name will be provided, for example BL1_3057. Three whole-rock granite samples were also included for trace element comparison purposes.

3.2. Microscopy and X-ray diffraction

Thin section studies on whole-rock samples utilised a combination of optical and scanning electron microscopy with energy dispersive X-ray spectroscopy (SEM–EDS). SEM–EDS analysis used the JEOL JXA-8500F (Hyperprobe) at the Deutsches GeoForschungsZentrum (GFZ) in Potsdam, Germany. Further petrographic analyses involved XRD analysis of whole-rock samples and clay separates (<2 μm). The XRD analyses were carried out on a Bruker Advance MK III X-Ray diffractometer with Bragg-Brentano geometry and CuKα radiation, operated at 40 kV and 30 mA at a scanning rate of 1 min/step and 0.05°/step. The samples were prepared for separation of the clay fraction by gently crushing the rocks to sand size, followed by disaggregation in distilled water using an ultrasonic bath. To ensure no detrital contamination, samples were centrifugally separated for

different size fractions and analysed with XRD using the above parameters. Samples showing evidence of contamination were either excluded from analysis or separated to finer micron fractions. Following XRD analysis of air-dried samples, the oriented clay-aggregate mounts were placed in an ethylene–glycol atmosphere at 30–40 °C overnight prior to additional XRD analysis. To determine illite content in illite–smectite mixed-layer clays, the method of differential two-theta (°Δ2θ) was used. This technique utilises the angular difference (°Δ2θ) between 001/002 and 002/003 peaks for ethylene-glycolated samples and estimates illite percentage with an analytical error of ±5%. A more detailed review of this method can be in found in Moore and Reynolds (1997).

3.3. Oxygen and hydrogen stable isotopes

Illitic clay minerals were analysed for their stable isotope ($\delta^{18}O$ and δD) compositions. Oxygen was extracted from illitic clays for isotope analyses using a CO_2-laser and BrF_5 (Sharp, 1990). Oxygen isotope values are reported in per mil relative to V-SMOW and normalised to the international quartz standard (NBS-28) using a value of 9.6‰. Replicate values for NBS-28 quartz (n = 6) analysed with the samples had values that varied by less than 0.2‰. UWG-2 garnet standard was run as an unknown and had a value of 5.8‰ with a variation of <0.1‰ per sample batch. Samples and standards were heated overnight in a muffle furnace to 170 °C prior to loading into the vacuum extraction line to remove any adsorbed water. The samples were then evacuated for approximately 6 hours and left overnight in a vapour of BrF_5. Blank BrF_5 was run until the yield was less than 0.1 micro moles oxygen. Oxygen was passed through a fluorine getter (in-line Hg diffusion pump) and converted to CO_2 by a graphite furnace; yields were recorded and CO_2 analysed on a Geo20–20 mass spectrometer at the GNS Laboratory, New Zealand. Hydrogen isotope analysis of

clays was similarly conducted at the GNS Laboratory using a HEKAtech high temperature elemental analyser coupled with a GV Instruments IsoPrime mass spectrometer. All samples were placed in 100°C vacuum dessicator overnight before being weighted into silver capsules. Samples were then kept in a 120°C oven for a further 24 hours before being immediately transferred to a Costec zero blank auto-sampler while still hot. The auto-sampler is flushed with helium and left for 3–4 hours before samples are pyrolyzed at 1450°C and analysed in triplicate. Results are calibrated to international standards Hexatriacontane, Methyl Ecosanate, NBS22, IAEA–CH–7 and Cumarine, with reported δD values of –246.7‰, –187‰, –118‰, –100‰, and 82.3‰ respectively. NBS-30 biotite standard was run as an unknown and had a reported δD value of –66‰. All hydrogen isotope ratios are reported in per mil relative to V–SMOW and have an analytical uncertainty of ±2‰ (1σ).

3.4. ICP–MS

As this work follows on from Rb–Sr geochronology described in Middleton et al. (2014), all previously separated untreated, leachate and acid-leached residue aliquots were also analysed for trace elements. Illitic clay separates were leached for 15 min at room temperature in 1 *N* distilled HCl (Clauer et al., 1993). Leachate and residue were separated by centrifuging. The residue was rinsed repeatedly with milli-Q water, dried and reweighed. Separates were dissolved with a mixture of HF and nitric acids on a hotplate, then evaporated to dryness, refluxed twice with nitric acid and dissolved in 2 *N* nitric acid. Aliquots of the solutions were spiked with internal standards, diluted and analysed for trace elements on a Thermo X-series 1 quadrupole inductively coupled plasma mass spectrometer (ICP-MS) in the Radiogenic Isotope Laboratory at the University of Queensland (RIF, UQ). Whole-rock samples were dissolved using HF + HNO_3 in Teflon beakers on a hot plate. The dissolved

samples were converted to nitrates and spiked with a multi-element internal standard solution (^{6}Li, ^{61}Ni, ^{103}Rh, ^{115}In, ^{187}Re, ^{209}Bi and ^{235}U) in 2% HNO_3. Sample preparation and analytical procedures used were similar to those of Eggins et al. (1997), except that Tm was not used as an internal standard and duplicate low-pressure digestions of W-2, a US Geological Survey diabase standard, were used as the calibration standard. BIR-1, AGV1, AGV2 and G2 were run as unknowns. The ^{156}CeO/^{140}Ce ratio for the run was 0.016. Long-term precision (RSD) was based on duplicate analyses of the duplicate digestions of AGV1, whilst precision for the run was based on five duplicate analyses of W-2, which were better than 3% for most elements, except for Li, Zn, Mo, Cd, and Cs that ranged between 5% (Li, Cd and Cs) and 15% (Zn).

4. RESULTS

4.1. Clay mineralogy

4.1.1. Nappamerri Trough

Two different types of illite–smectite were identified from the Nappamerri Trough. All granite and most sediment-hosted illites are characterised by 001 peaks of ~10 Å and show minimal to no shift of peaks upon ethylene glycolation. This indicates >95% illite typical of R ≥ 3 Reichweite-type with long-range ordering. The remaining sediment-hosted illite–smectite (BL57_ 1748.94) show shifts in the 001 peak from 9.7–9.6 Å after glycolation, with a broad shoulder from 11–12 Å. Such XRD patterns reflect illite–smectite with 80–90% illite on the border of short-range and long-range ordering (R = 1 – R ≥ 3; Reynolds and

Hower, 1970; Moore and Reynolds, 1997). Samples from the Nappamerri Trough show a wide range of illite crystallinity values (IC values) from 0.38 to 1.12 with median of 0.58. IC values do not show a systematic decrease with depth but rather irregular distribution, which is atypical of sedimentary basins where a systematic decrease with depth is normally attributed to incremental temperature increase (Fig. 2; Perry and Hower, 1970; Merriman and Frey, 1999). A full list of IC values clay separates are reported in Table 1**.**

4.1.2. GMI Ridge

The 001 peak of the majority of illite–smectite samples from the GMI Ridge shows minimal change in symmetry and position following ethylene glycolation and thus represents long-range ordered illite (>95% illite; R ≥ 3). Clay fractions from Mer1_3144, however, have XRD patterns with a broad shoulder from 11–12 Å following ethylene glycolation and are likewise attributed to illite–smectite with 80–90% illite (R = 1–R ≥ 3). IC values from the GMI Ridge show a narrower range from 0.55 to 0.95, with a higher median value of 0.63 than that of Nappamerri Trough illites. Likewise, IC values of the GMI Ridge also show non-linear scatter with depth with no systematic distribution (Fig. 2).

4.2. Petrography

4.2.1. Granite

In thin section, the majority of granite samples examined show intense illitic alteration resulting in almost complete replacement of feldspars and primary mica, representing ≥ 50% of the whole-rock (Fig. 3a). Some accessory phases (identified with

SEM–EDS) similarly show intense alteration, as seen from varying replacement of primary zircon [$ZrSiO_4$]. These replacement textures commonly contain xenotime [$HREEPO_4$], + thorite [$ThSiO_4$] along partially metasomatised rims in illite-altered samples. Or as almost completely altered anhedral to subhedral zircon remnants intergrown with xenotime + thorite ± bastnaesite (Fig. 3b; [$LREE(CO_3)F$]) in fluorite- and illite-altered samples. Samples with pervasive alteration also exhibit illite as anastomosing veinlets commonly associated with hydrothermal Th-rich colloform bastnaesite, as identified with EDS (Fig. 3c). Analysis of highly altered samples with FEG–SEM reveals two generations of illite recognisable by grain size and morphology. One generation is distinguished by large (up to 100 μm), lath-shaped crystals with convoluted compositional zonation. A cross-cutting generation, however, shows no identifiable chemical zonation and forms fine needle-like grains (Fig. 4a & b; 1–2 μm). Other alteration products include ankerite–siderite (confirmed by XRD) rimmed by akaganeite [Fe(OH,Cl)] intergrown with tabular bastnaesite and fluorite. Quartz is found as primary subhedral and microcrystalline grains. The deepest sample (McL1_3749.1) shows less intense alteration of primary feldspars and mica, with no evidence of illite veining. Isolated examples of euhedral monazite [$LREEPO_4$] and coffinite [$U(SiO_4)_x(OH)_{4x}$] are also found in the least altered samples and likely represent primary mineral species.

4.2.2. Sediments

Sampled Warburton and Cooper Basin sediments (siltstone–sandstone) consist of undulose quartz, altered feldspar (orthoclase and plagioclase), carbonate phases (commonly ankerite, identified by XRD), illite–smectite, microcrystalline quartz, detrital mica, detrital zircon and dispersed organic particles in thin section. The majority of sediment-

hosted illite–smectite occurs as alteration products from the replacement of feldspars and mica or as minor grain-coatings.

4.3. Stable isotope chemistry and palaeotemperature estimations

4.3.1. Nappamerri Trough

Estimated fluid isotopic values were calculated using appropriate mineral–fluid fractionation equations assuming isotopic equilibrium during mineral precipitation (Yeh, 1980; Sheppard and Gilg, 1996). A full list of stable isotope data for illite samples is presented in Table 1. Estimated fluid isotopic values were calculated using palaeotemperatures acquired from previous vitrinite reflectance data (VR; Kantsler et al., 1978). Vitrinite reflectance data is commonly used to determine coal "rank" (Uysal et al. 1999). Rank expresses organic maturation, due to increases in temperature, and acts as a reliable geothermometer because of its resistance to retrograde metamorphism (Teichmüller and Teichmüller, 1986; Wolf, 1988). Maximum reflectance measurements ($R_o$max) are obtained from embedded samples in a standardised oil immersion and calibrated against Australian reflectance standards. $R_o$max values were interpolated and extrapolated from reflectance/depth profiles of Kantsler et al. (1978) and converted to random reflectance (R_o) using the equation of Ting (1978). Palaeotemperature estimates were calculated using the time-independent method of Barker and Pawlewic (1986) and have an error of ±20 °C. This method was chosen due to the limited influence of heating duration on thermal maxima recorded by organic material (Barker and Pawlewicz, 1986). Palaeotemperatures for granite-hosted illites were estimated using vitrinite reflectance data of sediments at stratigraphically

equivalent depths. An interpolated palaeogeothermal gradient of ~100 °Ckm^{-1} is obtained if estimated palaeotemperatures are plotted against depth (Fig. 5).

Most granite-hosted illites have $\delta^{18}O$ values from 1.2 to 2.7‰, while $\delta^{18}O$ values of almost all sediment-hosted clay minerals range from 4.9 to 9.7‰. One granite-hosted sample from the Big Lake 1 drill hole does, however, have an anomalously negative $\delta^{18}O$ value of –1.8‰. Most granite- and sediment-hosted samples exhibit δD values ranging from –110 to –83‰ and –121 to –86‰, respectively. Using oxygen and hydrogen isotope fractionation equations (Yeh, 1980; Sheppard and Gilg, 1996), we calculated fluid isotopic values for illitic clays. Granite-hosted samples vary from –5.6 to –0.2‰ for $\delta^{18}O$ and –115 to –74‰ for δD, whereas sediments-hosted samples give values of –5.3 to 4.2‰ and –105 to –75‰, respectively. Palaeotemperature errors of 20 °C propagate to a mean error of ±8% for calculated fluid isotopic values.

Two main populations (A and B) exist when all calculated δD and $\delta^{18}O$ fluid isotopic values are plotted in a δD–$\delta^{18}O$ diagram (Figure 6). These populations comprise stratigraphically shallower samples with average δD values of –86‰ (Pop. A) and deeper samples with more negative δD values (average = –112‰; Pop. B). An inverse relationship is evident when $\delta D_{mineral}$ or δD_{fluid} are plotted against depth (Fig. 7).

4.3.2. GMI Ridge

Analyses of sediment-hosted illites from the GMI Ridge show a relatively narrow range in $\delta^{18}O$ and δD values from 7.1 to 11.9‰ and –100 to –78‰, respectively. Calculated fluid isotopic values vary between –1.3 and 4.7‰ for $\delta^{18}O$ and from –81 to –59‰ for δD. Palaeotemperature errors propagate to a mean error of ±10% for calculated $\delta^{18}O$ and δD fluid isotopic values. The majority of samples exhibit a positive correlation between δD

and $\delta^{18}O$, seen following the high latitudinal basin fluid projection (Fig. 8). Unlike the Nappamerri Trough, VR values from the GMI Ridge give a lower palaeogeothermal gradient of ~42 °Ckm^{-1}, as seen in Figure 5.

4.4. Trace element data

4.4.1. Nappamerri Trough

Trace element concentrations were measured for untreated, leachate and acid-leached residue aliquots of illite samples and whole-rock granite samples from the Nappamerri Trough for comparison purposes (Table 2). Upper continental crust-normalised (UCC) REE patterns of whole-rock and representative illite samples are presented in Figure 9 (Taylor and McLennan, 1985). UCC-normalised diagrams of granite-hosted, acid-leached residue mimic that of the whole-rock pattern presenting marginally LREE-rich to flat patterns with pronounced negative Eu-anomalies (Fig. 9a – c). Larger grain size fractions (< 2 and 1–2 μm) show minor enrichment in LREE to flat normalised patterns, whereas finer size fractions (< 1 and < 0.5 μm) are relatively LREE depleted. Rare earth element patterns for residue separates that produced a ~86 Ma isochron (Middleton et al., 2014) are consistently marked by a prominent negative Ce-anomaly (Fig. 9b). Comparatively LREE-depleted patterns with little to no Ce-anomaly are produced for older untreated and leachate separates from the Moomba 72 and Big Lake 1 drillholes (Fig. 9d), which define a ~94 Ma isochron (Middleton et al., 2014). Thorium concentrations of residue separates are substantially higher than typical basinal illite (Rousset and Clauer, 2003) and account for ~50% of whole-rock Th, as seen in Table 2. An estimation of 50% is based on the observation that ≥ 50% of the granitic samples are altered to illite. UCC-normalised trace element diagrams similarly show acid-leached

residue with comparable to elevated Th concentrations relative to unaltered granite (Fig. 9e). Additionally, leachate separates from Moomba 72 show distinctively higher concentrations of incompatible elements (e.g. Li, Be, Cr, Co, Ni and Pb) compared to leachates from other drill holes and unaltered granite. Middleton et al. (2014) noted that geologically significant ages were predominantly provided by isotopically resistant acid-leached residue aliquots. As such, only these will be considered in the following section to deduce prevailing physico-chemical conditions during hydrothermal events. Trace element concentrations of acid-leached residue are correlated with calculated fluid stable isotopic values. The δD values exhibit positive trends when plotted against Zr/Hf, Gd/Lu and Th concentrations of Nappamerri Trough illite (Fig. 10a – c). A positive relationship is also evident between Y/Ho and estimated palaeotemperature indicating dependency of trace element behaviour in hydrothermal fluids on temperature (Fig. 10d). Negative trends are evident when $\delta^{18}O$ fluid isotopic values are plotted against ΣREE and Th (Fig. 10e and f).

4.4.2. GMI Ridge

Acid-leached residues from the GMI Ridge all show MREE-poor REE patterns with some presenting minor LREE enrichment (Fig. 11a). Leachates produce highly MREE-enriched patterns with marginal to prominent negative Eu-anomalies and minor negative Y-anomalies (Fig. 11b). To a lesser extent than that seen in the Nappamerri Trough, calculated fluid stable isotopic values of GMI Ridge acid-leached illite also correlate with trace element data, as seen from positive and negative correlations when plotting $\delta^{18}O$ versus Y/Ho and δD versus La/Lu, respectively (Fig. 12a & b). A positive correlation is also seen between ΣREE and Gd/Lu (Fig. 12c). A full list of trace element data can be found in Table 3.

5. DISCUSSION

5.1. Illite authigenesis and its correlation with vitrinite reflectance

5.1.1. Nappamerri Trough

The Nappamerri Trough (Fig. 1b) has experienced multiple relatively high temperature (>170 °C) fluid flow events, as seen from the wide distribution of long-range ordered illite (R ≥ 3) (Pollastro, 1993). This resulted in several generations of illite precipitation with lath (>100 μm) to needle-like (1–2 μm) morphologies that may reflect decreasing water/rock ratios, respectively (Fig.4a & b; Uysal et al., 2000b). Episodic fluid influx was also noted by Middleton et al. (2014) who reported isochron ages of ~128, ~94 and ~86 Ma produced by ^{40}Ar–^{39}Ar, ^{87}Rb–^{87}Sr and ^{147}Sm–^{143}Nd dating of illite crystallites.

Vitrinite reflectance is proven to record maximum temperature of palaeothermal events (Barker and Goldstein, 1990; Uysal et al., 2000a). In diagenetic environments where temperature and vitrinite reflectance increase with depth, illite crystallinity values and expandability similarly show proportional decrease with depth (Perry and Hower, 1970; Merriman and Frey, 1999; Środoń, 2009). Such correlations are not well developed in the Warburton–Cooper basin system, as seen from variable illite crystallinity values and atypically high palaeotemperatures based on VR data (Fig. 2). This is evident in the Nappamerri Trough, where VR values correspond to estimated palaeotemperatures between 225 °C (2453.5 m) and 295 °C (3012 m), well above temperatures indicated by the IC values of ~0.56 (~175 °C; Merriman and Frey, 1999). Such extreme estimated

palaeotemperatures and associated palaeogeothermal gradient (Fig. 5; 100 °Ckm^{-1}) may reflect emplacement of the Carboniferous granite and/or a sudden influx of hydrothermal fluids over a short time period (Uysal et al., 2000a). Thermal modelling by Deighton and Hill (1998) showed that Cooper Basin hydrocarbons experienced maturation–expulsion into the dry-gas zone during a thermal maximum between 100 and 85 Ma; however, the cause of this thermal event was unknown. Therefore, high VR estimated temperatures, independent of IC values, may derive from the episodic Cretaceous hydrothermal events dated by Middleton et al. (2014), possibly in combination with latent heat associated with the BLS granite.

A similar variability of IC values with depth was seen in the Mt Isa Basin, Australia, and was attributed to factors in addition to temperature (Uysal et al., 2004; Golding et al., 2006). Other factors affecting illitisation, and resultant illite crystallinity, include potassium availability (Pearce et al., 1991), time (Hillier and Clayton, 1989) and water/rock ratio (Uysal et al., 2000a; Uysal et al., 2004). As IC values are associated with unusually high VR estimated palaeotemperatures, it is unlikely that illitisation occurred over a prolonged period and thus took place as a transient process (Uysal et al., 2000a and references therein). The irregular pattern of IC value increase with depth may, therefore, relate to variations in potassium supply and water/rock ratio. Granitic samples hosting illite-rich veins and pervasive illitic alteration, likely experienced high water/rock ratios with high potassium activities. Higher IC values (1.09; Mb1_2717.5 m) from some sediment-hosted samples, however, could reflect a reduced water/rock ratio (as seen from the $\delta^{18}O$ isotopic record) that inhibited the supply of potassium required for illitisation.

5.1.2. GMI Ridge

Illite (R ≥ 3) from GMI Ridge sediments likely formed from alteration of detrital feldspars and micas during the Carboniferous (323.3 ± 9.4 Ma) and Late Triassic (201.7 ± 9.3 Ma) hydrothermal events reported by Middleton et al. (2014). These hydrothermal regimes were characterised by somewhat lower palaeotemperatures (~165–195 °C) and significantly lower palaeogeothermal gradients (~42 °Ckm^{-1}) compared to the Nappamerri Trough, as seen from Fig. 5. This could suggest that while elevated Carboniferous and Late Triassic thermal regimes affected the entire basin system, the Cretaceous thermal event was most significant in the Nappamerri Trough. Less intense thermal regimes are similarly reflected by the higher average IC value of 0.63 and IC values as low as 0.73 at depths of 3895 m on the GMI Ridge. Lower IC values normally compatible with higher temperatures are counter-intuitively found at shallower depths indicating authigenesis was controlled by factors in addition to temperature.

Almost complete alteration of K-rich detrital phases (K-feldspar and mica) to illite–smectite and microcrystalline quartz is seen in thin section and indicates an active local supply of K^+ available for illitisation. However, the paucity of these minerals within certain GMI Ridge sediments suggest the supply was locally limited and thus, decreased the rate of illitisation. The restricted distribution of illite in areas of selected alteration of K-rich detrital phases may further suggest a substantially lower water/rock ratio limiting the flux of K-rich fluids and causing a 'lag' in the rate of illitisation (Pearce et al., 1991). This implies that erratic variations in IC values along the GMI Ridge may stem from localised variations in water/rock ratio.

5.2. Stable isotopes

5.2.1. Nappamerri Trough

Regardless of error from VR temperatures (±8%), calculated fluid values are consistent with illite precipitation from evolved high-latitudinal Cretaceous meteoric waters (Veevers, 1984). It is unlikely these values suffered post-formational isotopic exchange during younger fluid flow events. If this were the case, ^{40}Ar–^{39}Ar heating spectra for these samples would have shown disturbance and recorded chronologically meaningless data, which was not noted by Middleton et al. (see Figures 5–8; 2014). A typical J-shaped evolution away from the meteoric water line (MWL), shown by Scenario I (Figure 6), is unlikely. This would imply involvement of meteoric waters (~ $\delta^{18}O$ = –16.5‰ and δD = –120‰) with similar values to diagenetic fluids (~ $\delta^{18}O$ = –17.5‰ and δD = –125‰) of the Otway and Gippsland basins of south Australia that were at substantially higher latitudes during the mid-Cretaceous (Gregory et al., 1989).

The presence of two populations for Nappamerri fluid values (Scenario II; Figure 6) more likely results from an evolving meteoric fluid with a divergent trajectory away from Cretaceous meteoric water compositions (~ $\delta^{18}O$ = –13‰ and δD = –90‰) (cf. Uysal et al., 2011b). Less negative fluid δD values shown by samples along the upturned trend (Population A) are compatible with isotopic exchange with hydrogen-rich minerals under low water/rock ratios (Fig. 6; Yardley et al., 1991; Uysal et al., 2000c). In contrast, a downturned isotopic trend to more negative fluid δD and somewhat more positive fluid $\delta^{18}O$ values for population B may indicate a decoupling of the hydrogen and oxygen isotopic systems at depth (Fig. 6). The expulsion of hydrocarbons during the lower Cretaceous may offer an explanation, as organic material acts as a substantial source of isotopically light hydrogen (Ziegler et al., 1994; Polya et al., 2000).

Previous studies have shown that hydrothermal interaction processes are efficient drivers of organic maturation during which H-exchange can occur between

hydrocarbons and water via reversible equilibrium fractionation (Didyk and Simoneit, 1989; Simoneit, 1992; Schimmelmann et al., 2006; Reeves et al., 2012). More negative mineral and fluid δD values with depth may suggest that increasing fluid temperatures resulted in more intense alteration–maturation of organic matter. This would have contributed a larger proportion of D-depleted hydrogen to the fluid phase prior to the alteration of granite and precipitation of illite (Fig. 7; Ziegler et al., 1994; Girard et al., 2002). This suggestion is also compatible with widespread hydrocarbon maturation within the Cooper and Eromanga Basins, correlated with an anomalous thermal event in the Late Cretaceous (Deighton and Hill, 1998). Slightly more positive fluid $\delta^{18}O$ values of population B with depth cannot realistically result from decreasing temperature, as vitrinite reflectance data show typical increasing palaeotemperatures with depth (Fig. 5; Kantsler et al., 1978). A possible scenario can be modelled using the integrated water/rock ratio equation of Taylor (1997):

$$\frac{w}{r} = \ln\left[\frac{\delta^{i}_{H_2O} + \Delta - \delta^{i}_{rock}}{\delta^{i}_{H_2O} - (\delta^{f}_{rock} - \Delta)}\right]$$

where $\Delta \approx 1000\ln\alpha = 2.39\text{x}10^{6}\text{ x } T^{-2} - 3.76$ or the illite–water fractionation factor (Sheppard and Gilg, 1996), *i* is the initial value and *f* is the final value after exchange. The illite–water fractionation factor of Sheppard and Gilg (1996) is used due to the pervasive nature of illitisation, which composes ~50% of the whole-rock. Temperatures for the calculation of fractionation factor mimic those recorded by vitrinite reflectance. If plausible assumptions are made for initial fluid and granite $\delta^{18}O$ values, then δ^{f}_{rock} or hypothetical illite values can be modelled by rearranging the above equation for a range of water/rock ratios, as seen in Figure 13 (calculations seen in Appendix A):

$$\delta^{f}_{rock} = -\left[\left[\frac{\delta^{i}_{H_2O} + \Delta - \delta^{i}_{rock}}{e^{w/r}}\right] - \delta^{i}_{H_2O}\right] - \Delta$$

A granite $\delta^{18}O$ value of 10‰ was estimated from a range of similarly aged, S- and I-type granites from eastern New South Wales, Australia (O'Neil et al., 1977). An initial $\delta^{18}O$ fluid value of –12‰ was taken from authigenic illites of the Gunnedah Basin of similar age (84 and 96 Ma) and latitude (~30°S; Uysal et al., 2011b). Assuming negligible detrital phase contamination, a more plausible explanation is that more positive $\delta^{18}O$ fluid values in the down-turned trajectory result from fluid-rock interaction with ^{18}O-rich phases under lower water/rock ratios. This is evident in Figure 13 as authigenic illites transition to more positive $\delta^{18}O$ values from environment A_I to A_{II} due to precipitation from higher temperature fluids under lower water/rock ratios. A pattern of more negative δD and more positive $\delta^{18}O$ values with depth indicates isotopic exchange with hydrogen and oxygen from different reservoirs. Variations in hydrogen appear to reflect temperature-dependent fluid–rock interaction with organics, while variations in $\delta^{18}O$ values are largely affected by varying water/rock ratios during interaction with silicate-rich rocks.

Anomalously negative $\delta^{18}O$ values in the Big Lake drill holes (Fig. 6) are likely due to fluid–rock interactions under considerably higher water/rock ratios (cf. Uysal et al., 2000c); as modelled in Figure 13 by comparison of environments A_I and B_I. Environment B_I was only modelled at water/rock ratios just past unity as episodic thermal events have limited quantities of heat to drive hydrothermal convection (Taylor, 1997). More positive $\delta^{18}O$ values of some sediment-hosted clays are consistent with extensive oxygen isotopic exchange, under lower water/rock ratios, between lower temperature hydrothermal fluids and sedimentary assemblages, as seen in geothermal systems of extensional environments (Truesdell and Hulston, 1980).

5.2.2. GMI Ridge

Calculated $\delta^{18}O$ fluid isotopic values for GMI Ridge illitic clays are similar to those of formation waters of sedimentary basins (Clayton et al., 1966). A positive correlation between $\delta^{18}O$ and δD tracks that of an evolved basinal fluid, of mid- to high-latitudinal meteoric origin, experiencing broad isotopic exchange with ^{18}O-rich sediments away from the meteoric water line (Fig. 8). This explanation is consistent with south-west Queensland's mid to high latitudinal position during the Late Triassic and Carboniferous (Veevers, 2004). Alternatively, a large ^{18}O shift in fluid values away from the MWL may result from extensive oxygen isotopic exchange of hot meteoric waters with surrounding rocks; characteristic of open, geothermal systems (Truesdell and Hulston, 1980). Extrapolating to the MWL gives expected fluid values of approximately –75‰ (δD) and –11‰ ($\delta^{18}O$) that are consistent with Australia's lower palaeolatitude in the Triassic (Veevers, 2004), compared to Cretaceous illite samples of the Nappamerri Trough.

Samples with near uniform δD likely result from minimal isotopic exchange with anhydrous silicate minerals, allowing the hydrogen isotope composition of the fluid to dominate the hydrothermal system (Sheppard, 1986) Varying $\delta^{18}O$ values, however, may result from localised variations in water/rock ratio, as seen from Nappamerri Trough illites (above). The least negative δD value, given by sample T7_3032, may originate from precipitation during fracture-guided fluid-flow under low water/rock ratio conditions permitting substantial isotopic exchange with hydrogen-rich minerals (Goldfarb et al., 1991; Yardley et al., 1991).

5.3. Trace element data

5.3.1. Nappamerri Trough

Differential mobility of trace elements, such as REE, in hydrothermal solutions depends on parameters such as fluid composition and redox state (Wood, 1990; Bau, 1991). The presence of negative Ce-anomalies throughout UCC-normalised patterns from ~86 Ma residues of illites from the Nappamerri Trough is testament to this, and allows distinction from ~94 Ma residues without consistent Ce-anomalies (Fig. 9b) (Middleton et al., 2014). Such anomalies can develop from a change in valency of Ce (Ce^{3+} to Ce^{4+}) in oxidising conditions to form insoluble cerianite (CeO_2) that will fractionate from the remaining, more mobile REE^{3+} (Bau, 1991; Bau and Möller, 1992; Uysal et al., 2011a). Leachates and untreated separates from Moomba 72 can similarly be differentiated by their anomalous UCC-normalised REE and trace element patterns (Fig. 9e). As Moomba 72 residue samples are not anomalous, trace element composition for untreated separates must relate to the contribution from the leachable phases. Unusually low LREE concentrations may relate to precipitation of leachable phases from compositionally different fluids. Furthermore, as Moomba 72 leachates have unusually high concentrations of lithophile and siderophile elements (Li, Be, Cr, Co, Ni and Pb), hot evolved meteoric fluids may have interacted with alkaline mafic rocks prior to precipitation of leachable phases. Possible elemental sources include undiscovered mafic enclaves of the BLS granite or the Warburton Basin "Jena Basalt" that was interpreted to have a "within-plate" continental geochemical affinity (Boucher, 2003).

Stable isotope results suggest more negative δD values with depth derive from a greater contribution of organic-derived hydrogen at higher temperatures. Therefore, positive correlations between Gd/Lu and δD may indicate temperature-dependent preferential mobilisation of lighter REE, typical of Cl, carbonate or fluorine-rich fluids (Luo and Byrne, 2001; Luo and Byrne, 2004; William-Jones et al., 2012). The reason for the two populations seen in Figure 10b is not completely understood but may reflect mobilisation of REE by

separate fluids through chemically distinctive rocks. The presence of hydrothermal fluorite indicates it is unlikely that REE were mobilised by fluoro-complexes. This results from the strong affinity of Ca^{2+} for F^{-} buffering the concentration of ligands available for complexation in solution (Salvi and William-Jones, 1990; Salvi and William-Jones, 1996; Merriman and Frey, 1999). Rare earth elements were more likely mobilised via chlorine-complexation, due to the occurrence of Cl-rich akageneite and the higher stability of Cl complexes over other mobilising ligands in hydrothermal systems (William-Jones et al., 2012). Mobilisation by chlorine-complexation also accounts for the positive correlation seen between Y/Ho and estimated palaeotemperature (Fig. 10d). This is due to the higher stability complex of $HoCl^{2-}$over YCl^{2-} allowing the preferential mobilisation of Ho^{3+} at lower temperatures (Luo and Byrne, 2001).

Well-defined negative correlations between $\delta^{18}O$ and REE or Th may reflect the degree of alteration and changing water/rock ratio (Fig. 10e & f). These correlations can similarly be modelled by comparing hypothetical environments A_I (REE-poor) and B_I (REE-rich) in Figure 13. Under lower water/rock ratios at point A_I (1), the granite experienced less intense alteration, which resulted in lower concentrations of Th and REE being leached and incorporated into illites with *less* negative $\delta^{18}O$ values (–1‰). However, by increasing the water/rock ratio (3) and degree of alteration (point B_I) authigenic illite has *more* negative $\delta^{18}O$ values (–6‰) and higher concentrations of Th and REE were mobilised in solution. Granite samples in this study, which also experienced higher water/rock ratio alteration are characterised by relatively low illite $\delta^{18}O$ values and pervasive illite formation that comprises ~50% of altered rock mass. It should be noted that very altered granite samples (MB1_2857.4; Fig. 3a) contain the highest concentrations of Th, with illite accounting for ~40–50% of the total budget, while the remaining Th likely resides predominantly in accessory phases, such as bastnaesite (Fig. 3c). Uranium concentrations are, however, similar

in altered and unaltered samples. While it is not fully understood, this may suggest that U was relatively immobile due to reducing conditions or mineral-surface adsorption (Skirrow et al., 2009). Thorium-enriched illite suggests that illitising hydrothermal fluids were able to leach and/or mobilise substantial concentrations of Th from elsewhere within the granitic body. Alternatively, as unaltered BLS granite hosts lower Th content than its altered counterpart, Th may have been mobilised from the surrounding country-rock. This seems likely as preceding uplift and glacial erosion of the granite lead to shedding of HPE-enriched detritus into surrounding lithologies, such as the "Tirrawarra Conglomerate" (Meixner et al., 1999). As such, episodic influxes of Cretaceous hydrothermal fluids carrying high concentrations of Th, could actively affect the budget of heat-producing elements in the BLS granite. This phenomenon is compatible with the work of Martin (2006), who suggested that unusually high concentrations of HFSE, REE and HPE in anorogenic granites relate to protracted interaction of fenitising hydrothermal fluids with the crust during magma emplacement.

Samples with relatively depleted Th content are similarly coupled with the lowest δD values, attributed to interaction with isotopically light organic-rich material (Fig. 10c; Polya et al., 2000). Correlations between Th and δD may simply reflect lower degrees of alteration and increasing thermal degradation of organics at systematically greater depths. This is also seen from positive correlations between Zr/Hf and δD, as more intense alteration will result in greater concentrations of Zr being liberated from Zr-bearing phases into solution (Fig. 10a). Variations in Zr/Hf ratios likely reflect fractionation of the geochemical twin pairs (Zr–Hf) from each other due to differences in aqueous chemical complexation and electron structure (Bau, 1996).

5.3.2. GMI Ridge

Illite samples associated with Late Triassic and Carboniferous events from the GMI Ridge are chemically differentiable from those formed during the Cretaceous in the Nappamerri Trough (Middleton et al., 2014). This is seen from the presence of MREE-depleted UCC-normalised patterns of residue separates, whilst leachates present MREE-rich patterns with negative Eu- and Y-anomalies (Fig. 11a & b). Differing REE patterns for these separates may represent variable physico-chemical conditions during fluid-rock interaction associated with Carboniferous and Late Triassic thermal events for residues and leachates, respectively (Middleton et al., 2014). The pronounced negative Eu-anomaly may result from fluid-mineral interaction with Eu-depleted phases, such as muscovite, prior to precipitation of the leachable phase. Negative Y-anomalies could also suggest REE mobilisation by (bi)carbonate-rich hydrothermal solutions where Y acts as a light pseudolanthanide. The term "pseudolanthanide" refers to the ability of Y to act similarly to either light or HREE depending on fluid composition (Bau and Dulski, 1995).

The GMI Ridge experienced a substantially different fluid flow regime compared to the Nappamerri Trough. This may reflect interaction of hydrothermal fluids with markedly different lithologies with less systematic variations in water/rock ratio and temperature. As such fewer correlations could be made between trace element concentrations and calculated fluid isotopic values. Moreover, identified correlations may indicate hydrothermal fluids in the GMI Ridge had differing chemistries, which differentially mobilised trace elements. The negative correlation between La/Lu and δD for residue separates may indicate preferential mobilisation of HREE in a cooling fluid experiencing minor isotopic exchange with hydrogen-bearing phases (Fig. 12c). This is similarly seen from a positive correlation between REE and Gd/Lu (Fig. 12b). This observation is compatible with preferential mobilisation of HREE in lower temperature, near neutral to basic fluids rich in fluorine or (bi)carbonate ligands (Bau and Dulski, 1995; Rolland et al., 2003; William-

Jones et al., 2012). Mobilisation of HREE by fluorine complexation rather than (bi)carbonate is consistent with a positive correlation between Y/Ho and $\delta^{18}O$, which results from Y acting as a heavy pseudolanthanide in progressively evolving/cooling F-rich fluids (Fig 12a). The abundance of such ligands may derive from mixing of deep-circulating evolved meteoric fluids with concurrent orthomagmatic fluids sourced during late Carboniferous emplacement of the Big Lake Suite granite (Gatehouse et al., 1995; Uysal et al., 2011b; Middleton et al., 2014).

5.4. Significance and implications of thermal and fluid flow history

5.4.1. Nappamerri Trough

Stable isotope and mineralogical data imply episodic influx of evolved meteoric water under variable water/rock ratio conditions, resulting in intense alteration of the BLS granite. This scenario is compatible with published evidence inferring an extensional tectonic environment in the mid Cretaceous (Deighton and Hill, 1998; Mavromatidis, 2008; Bryan et al., 2012; Cook et al., 2013) and consistent with previous Sm–Nd, Rb–Sr and Ar–Ar dating of illite separates (Middleton et al., 2014). Localised extensional tectonism stems from continent-wide transmission of tensional stress to thermally and mechanically weaker regions of the continental crust (Coblentz and Sandiford, 1994; Friedmann and Burbank, 1995; Armitage and Allen, 2010; Müller et al., 2012). Such stress originated from a >2500km long episodic rifting event that affected much of the Eastern Australian margin and is associated with formation of the Whitsundays Large Igneous Province (100 – 90 Ma; O'Sullivan et al., 1995) as well as opening of the Tasman Sea (~84 Ma; Veevers et al., 1991). Rifting and related fluid flow produced an extremely high geothermal gradient (~100 $°Ckm^{-1}$) that was

restricted to the Nappamerri Trough with little or no affect on the structurally high GMI Ridge, which maintains Carboniferous and Late Triassic isotopic records (Middleton et al., 2014). Similarly high palaeogeothermal gradients have been recorded in amagmatic continental rift settings of the Upper Rhine Graben, France (up to 120 °Ckm^{-1}; Werner and Doebl, 1974) and Bowen Basin, Australia (up to 132 °Ckm^{-1}; Uysal et al., 2000a) with the latter also being attributed to episodic convective heat transfer in hydrothermal conditions. An elevated Cretaceous thermal regime in conjunction with low δD values suggest high temperature interaction with organics and may offer a potential explanation for the maturation and expulsion of hydrocarbons that formed Australia's largest on-shore petroleum reserves (Deighton and Hill, 1998; APPEA, 2003).

Episodic fluid flow is also shown from trace element data as all samples plotting on a ~86 Ma isochron have discrete negative Ce-anomalies indicating an oxidising environment. In contrast, those forming ~94 Ma isochrons do not, implying different, more anoxic physico-chemical conditions during preceding hydrothermal circulation. Moreover, Middleton et al. (2014) also noted that the illites from the ~86 Ma event are predominantly found at shallower depths (~2850 m) implying that prior ~94 Ma fluid flow substantially reduced permeability at greater depths, and thus limited later fluid flow to more permeable, shallower fracture networks. Multiple Cretaceous fluid flow events also had profound effects on the heat-producing nature of the BLS granite and caused substantial hydrothermal enrichment in the heat-producing element Th.

5.4.2. GMI Ridge

Palaeotemperature data indicate the structurally high GMI Ridge experienced less intense thermal regimes with palaeogeothermal gradients of ~42 °Ckm^{-1}, and was not

affected by the Cretaceous event. This is compatible with previous geochronology that recorded only Carboniferous (323.3 ± 9.4 Ma) and Late Triassic (201.7 ± 9.3 Ma) ages (Middleton et al., 2014) from illite samples along the GMI Ridge. This is also shown from stable isotope data indicating the involvement of isotopically different hydrothermal fluids consistent with evolved basinal fluids of meteoric origin. An influx of basinal fluids in the Carboniferous marks the extension of the Warburton Basin, as seen from normal faulting along the "Moomba High" (Apak et al., 1995), and intrusion of the BLS granite dated at 323 ± 5 Ma (Gatehouse et al., 1995). A similar scenario was also postulated by McLaren et al. (2006) who saw disturbed $^{40}Ar/^{39}Ar$ results for K-feldspar from the BLS and attributed this to circulation of basinal fluids in an extensional setting. Localised thermal and tectonic perturbations may relate to widespread extensional tectonism that affected much of Queensland resulting in the formation of basinal depocentres (Van Heeswijck, 2010) and emplacement of multiple silicic igneous bodies in the Connors–Auburn Province (Allen et al., 1998; Donchak et al., 2013).

An elevated thermal regime in the Late Triassic similarly involved the ingress of basinal fluids of meteoric origin. Fluid flow most likely derived from an elevated thermal regime during formation of the Eromanga Basin (Mavromatidis, 2008). Such an event is coincident with extensional tectonism that affected large areas of eastern Queensland towards the end of the Triassic (Cook et al., 2013). This formed multiple, small fault-bounded sedimentary basins across the Bowen Basin (Fielding, 1996; Uysal et al., 2001) and was accompanied by large-scale silicic magmatism in the New England Fold Belt of south-east Queensland (Stephens, 1991).

5.5. Implications for the formation of highly radioactive granites and influence on enhanced geothermal system exploration

A-type or anorogenic granites can have especially high concentrations of heat-producing elements if their parent melt derives from a metasomatised and previously enriched crustal source (Martin, 2006; Bea, 2012). Crustal enrichment results from multiple influxes of mantle-sourced, volatile-rich fluids. Such fluids can escape from a rising asthenospheric plume in an anorogenic setting, leach high-field strength elements and REE from the surrounding rock and enrich areas of the lower crust (Woolley, 1987; Martin, 2006).

Vein and authigenic mineral phases sampled from the Warburton–Cooper–Eromanga basins record multiple tectonic events that allowed hydrothermal fluid circulation (Middleton et al., 2014). Illite specifically records five events in the Carboniferous, Late Triassic and Cretaceous. The BLS granite is pervasively altered, with illite comprising ~50% of the rock mass. Trace element analyses of illite samples show that residue fractions have Th and U concentrations up to 93 ppm and 25 ppm, respectively. In some samples, illite contributes up to ~50% of the heat-producing nature of the granite. This implies that fluids capable of altering the granite were laden with radiogenic elements potentially leached from the surrounding country-rock and granite. The implications of this observation are two-fold. The first is that under certain hydrothermal conditions, Th is substantially more mobile than previously thought. The second is that episodic hydrothermal mobilisation of heat-producing elements may offer an alternative, metasomatic origin for the unusual enrichment of the BLS in radiogenic elements. Analysis of secondary mineral phases clearly offers a potential tool during exploration for enhanced geothermal systems. Conducting geochemical and geochronological analysis on authigenic illite can provide evidence for episodic fluid flow and whether fluids were capable of mobilising radiogenic elements. Therefore, if an anorogenic granite is highly altered and has experienced multiple periods of hydrothermal

interaction with radiogenic element-rich fluids, it may represent a high-priority target for geothermal energy utilisation.

6. CONCLUSIONS

This study utilised mineralogical, trace element and stable isotopic analyses of authigenic illite to chemically differentiate successive hydrothermal events in the Warburton–Cooper basins, previously dated by Middleton et al. (2014). Analyses of illites from the GMI Ridge, in conjunction with previous VR studies (Kantsler et al., 1978), record Carboniferous and Late Triassic thermal events (~42 °Ckm^{-1}). These perturbations involved basinal fluids of evolved meteoric origin that interacted with the country rocks under low water/rock ratio conditions. Rare earth element studies further show that while the Late Triassic event had elemental distribution indicative of (bi)carbonate-rich solutions, the Carboniferous regime was characterised by fluorine-rich fluids that may derive from the involvement of orthomagmatic magmatic fluids.

In contrast, samples from the Nappamerri Trough indicate episodic circulation of evolved meteoric waters under variable water/rock ratios and high geothermal gradients in the Cretaceous (~100 °Ckm^{-1}). The influx of moderate-temperature hydrothermal fluids had a significant effect on the surrounding geology leading to the maturation–expulsion of hydrocarbons as well as a substantial enrichment of the BLS granite in Th. However, to fully understand the enrichment and mobility of heat-producing elements in this system, further research on primary granite chemistry and accessory phases is required. Our work, in tandem with previous geochronology (Middleton et al., 2014) provides additional temporal and chemical constraints on the formation of two of Australia's more prolific energy resources.

Furthermore, by combining mineralogical, chemical and previous chronological analyses (Middleton et al., 2014), this study provides the most comprehensive and holistic record of the thermal, tectonic and fluid flow evolution of one of the world's more enigmatic basin systems.

Acknowledgments

The authors acknowledge the Government of South Australia and Geodynamics Ltd. for granting permission to sample core. We thank Dr. Yue-xing Feng, Dr. Ai Duc Nguyen, Dr. Hans-Jürgen Förster and Dr. Dieter Rhede for their help with analytical work and technical assistance. Special thanks go to Turgay Demir for his assistance during sample preparation. Microscopy was undertaken at Deutsches GeoForschungsZentrum, Potsdam, as part of a collaborative research agreement between this Federal Research Institute and The University of Queensland, Australia. F. Longstaffe and two anonymous reviewers are thanked for thoughtful and constructive reviews of the manuscript.

References

Alexander, E. M., 1998. Lithostratigraphy and environments of deposition. In: Gravestock, D. I., Hibburt, J., and Drexel, J. F. Eds.)*Petroleum Geology of South Australia, Cooper Basin*. South Australian Department of Primary Industries and Resources, **4**, 69–116. Adelaide.

Allen, C. M., Williams, I. S., Stephens, C. J., and Fielding, C. R., 1998. Granite genesis and basin formation in an extensional setting: The magmatic history of the Northernmost New England Orogen. *Aust. J. Earth Sci.* **45**, 875–888.

Apak, S. N., Stuart, F., Lemon, N. M., and Wood, G., 1997. Structural evolution of the Permian–Triassic Cooper Basin, Australia: Relation to hydrocarbon trap styles. *AAPG Bulletin* **81**, 533–555.

Apak, S. N., Stuart, W. J., and Lemon, N. M., 1995. Compressional control on sedimentation and facies distribution SW Nappamerri Syncline and adjacent Murteree High, Cooper Basin. *The APEA Journal* **35**, 190-202.

APPEA, 2003. *Development and Production Statistics*. Australian Petroleum Production and Exploration Association Limited, Canberra.

Armitage, J. J. and Allen, P. A., 2010. Cratonic basins and the long-term sibsidence history of continental interiors. *J Geol Soc London* **167**, 61–70.

Barker, C. E. and Goldstein, R. H., 1990. A fluid inclusion technique for determining maximum temperature in calcite and its comparison to the vitrinite reflectance geothermometer. *Geology* **10**, 1003–1006.

Barker, C. E. and Pawlewicz, 1986. The correlation of vitrinite reflectance with maximum temperature in humic organic matter. In: Buntebarth, G. and Stegena, L. Eds., *Paleogeothermics*. Springer-Verlag, New York.

Bau, M., 1991. Rare-earth element mobility during hydrothermal and metamorphic fluid-rock interaction and the significance of the oxidation state of europium. *Chem. Geol.* **93**, 219–230.

Bau, M. and Dulski, P., 1995. Comparative study of yttrium and rare-earth element behaviours in fluorine-rich hydrothermal fluids. *Contrib. Mineral. Petr.* **119**, 213–223.

Bau, M. and Möller, P., 1992. Rare Earth Element Fractionation in Metamorphogenic Hydrothermal Calcite, Magnesite and Siderite. *Mineral. Petrol.* **45**, 231–246.

Bau, M., Romer, R. L., Lüders, V., and Dulski, P., 2003. Tracing element sources of hydrothermal mineral deposits: REE and Y distribution and Sr-Nd-Pb isotopes in fluorite from MVT deposits in the Pennine Orefield, England. *Miner. Deposita* **38**, 992–1008.

Bea, F., 2012. The sources of energy for crustal melting and the geochemistry of heat-producing elements. *Lithos* **153**, 278–291.

Boucher, R. K., 2003. The influence of deep-seated structures on hydrocarbon accumulation in the Cooper and Eromanga Basins. PhD, University of South Australia.

Bryan, S. E., Cook, A. C., Allen, C. M., Siegel, C., Purdy, D., Greentree, J. S., and Uysal, I. T., 2012. Early–mid Cretaceous tectonic evolution of eastern Gondwana: From silicic LIP magmatism to continental rupture. *Episodes* **35**, 142–152.

Chopra, P. and Wyborn, D., 2003. Australia's first hot dry rock geothermal energy extraction project is up and running in granite beneath the Cooper Basin, NE South Australia,

The Ishihara Symposium: Granites and Associated Metallogenesis. 43-45. Macquarie, Australia.

Clauer, N., Chaudhuri, S., Kralik, M., and Bonnotcourtois, C., 1993. Effects of experimental leaching on Rb–Sr and K–Ar isotopic systems and REE contents of diagenetic illite. *Chem. Geol.* **103**.

Clayton, R. N., Friedman, I., Graf, D. L., Mayeda, T. K., Meents, W. F., and Shimp, N. F., 1966. The origin of sline formation waters. *Journal of Geophysical Research* **71**, 3869–3882.

Coblentz, D. D. and Sandiford, M., 1994. Tectonic stresses in the African plate: Constraints on the ambient lithospheric stress state. *Geology* **22**, 831–834.

Cook, A. G., Bryan, S. E., and Draper, J. J., 2013. Post-orogenic Meoszoic basins and magmatism. In: Jell, P. A. (Ed.), *Geology of Queensland*. Geological society of Queensland, Brisbane.

Deighton, I. and Hill, A. J., 1998. Thermal and burial history. In: Gravestock, D. I., Hibburt, J., and Drexel, J. F. Eds., *Petroleum Geology of South Australia*. South Australia. Department of Primary Industries and Resources.

Didyk, B. M. and Simoneit, B. R. T., 1989. Hydrothermal oil of Guaymas Basin and implications for petroleum formation mechanisms. *Nature* **65–69**.

Donchak, P. J. T., Purdy, D. J., Withnall, I. W., Blake, P. R., and Jell, P. A., 2013. New England Orogen. In: Jell, P. A. (Ed.), *Geology of Queensland*. Geological Society of Queensland, Brisbane.

Eggins, S. M. W., J. D., Kinsley, L. P. J. M., G. E., Sylvester, P., McCulloch, M. T., Hergt, J. M., and Handler, M. R., 1997. A simple method for the precise determination of ≥ 40 trace elements in geological samples by ICPMS using enriched isotope internal standardisation. *Chem. Geol.* **134**, 311–326.

Fielding, C. R., 1996. Mesozoic sedimentary basins and resources in eastern australia – A review of current understanding, *Mesozoic Geology of the Eastern Asutralian Plate Conferene*. Geological Society of Australia, 43, 180–185. Brisbane.

Friedmann, S. J. and Burbank, D. W., 1995. Rift basins and supra-detachment basins: intracontinental extensional end-members. *Basin Res.* **7**, 109–127.

Gatehouse, C. G., 1986. The geology of the Waburton Basin in South Australia. *Aust. J. Earth Sci.* **33**, 161–180.

Gatehouse, C. G., Fanning, C. M., and Flint, R. B., 1995. Geochronology of the Big Lake Suite, Warburton Basin, northeastern South Australia, *Quarterly Geological Notes*. Geological Survey of South Australia, **128**, 8–16.

Gerard, A., 2006. The deep EGS (Enhanced Geothermal System) project at Soultz-sous-Forêts (Alsace, France). *Geothermics* **35**, 473–483.

Girard, J.-P., Munz, I. A., Johansen, H., Lacharpagne, J.-C., and Sommer, F., 2002. Diagenesis of the Hild Brent Sandstones, Northern North Sea: isotopic evidence for the prevailing influence of deep basinal water. *Journal of Sedimentary Research* **72**, 746-759.

Goldfarb, R. J., Newberry, R. J., Pickthorn, W. J., and Gent, C. A., 1991. Oxygen, hydrogen, and sulfur isotope studies in the Juneau gold belt, southeastern Alaska: constraints on the origin of hydrothermal fluid. *Econ. Geol.* **86**, 66–80.

Golding, S. D., Uysal, I. T., Glikson, M., Baublys, K. A., and Southgate, P. N., 2006. Timing and chemistry of fluid-flow events in the Lawn Hill Platform, Northern Australia. *Econ. Geol.* **101**, 1231-1250.

Gravestock, D. I. and Jensen-Schmidt, B., 1998. Structural setting. In: Gravestock, D. I., Hibburt, J., and Drexel, J. F. Eds.)*Petroleum Geology of South Australia, Cooper Basin*. South Australian Department of Primary Industries and Resources, **4**, 47–68. Adelaide.

Gregory, R. T., Douthitt, C. B., Duddy, I. R., Rich, P. V., and Rich, T. H., 1989. Oxygen isotopic composition of carbonate concretions from the lower Cretaceous of Victoria, Australia: implications for the evolution of meteoric waters on the Australian continent in a paleopolar environment. *Earth Planet. Sci. Lett.* **92**, 27–42.

Hillier, S. and Clayton, T., 1989. Illite / smectite diagenesis in Devonian lacustrine mudrocks from northern Scotland and its relationship to organic maturity indicators. *Clay Miner.* **24**, 181–196.

Kantsler, A. J., Cook, A. C., and Smith, G. C., 1978. Rank variation, calculated palaeotemps and understanding oil, gas occurrence. *Oil and Gas Journal* **Nov. 20**, 196–205.

Kuang, K. S., 1985. History and style of Cooper–Eromanga Basin structures. *Exploration Geophysics* **16**, 245–248.

Kyser, T. K., 2007. Fluids, basin analysis, and mineral deposits. *Geofluids* **4**, 238-257.

Longstaffe, F. J., 2000. An introduction to stable oxygen and hydrogen isotopes and their use as fluid tracers in sedimentary systems. In: Kyser, K. (Ed.), *Fluids and Basin Evolution*. Mineralogical Association of Canada, Ottawa.

Luo, Y.-R. and Byrne, R. H., 2001. Yttrium and rare earth element complexation by chloride ions at 25°C. *Journal of Solution Chemistry* **30**, 837–845.

Luo, Y.-R. and Byrne, R. H., 2004. Carbonate complexation of Yttrium and the rare earth elements in natural waters. *Geochim. Cosmochim. Acta* **68**, 691–699.

Marshall, V. J., 2014. Petrological, geochemical and geochronological characterisation of heat-producing granites. MPhil, University of Queensland.

Martin, R. F., 2006. A-type granites of crustal origin ultimately result from open-system fenitization-type reactions in an extensional environment. *Lithos* **91**, 125–136.

Mavromatidis, A., 2006. Burial/exhumation histories for the Cooper-Eromanga Basins and implications for hydrocarbon exploration, Eastern Australia. *Basin Res.* **18**, 351–373.

Mavromatidis, A., 2008. Two layer model of lithospheric compression and uplift / exhumation in an intracratonic setting: an example from the Cooper–Eromanga Basins, Australia. *International Journal of Earth Science* **97**, 623–634.

McLaren, S. and Dunlap, W. J., 2006. Use of $^{40}Ar/^{39}Ar$ K-feldspar thermochronology in basin thermal history reconstruction: an example from the Big Lake Suite granites, Warbruton Basin, South Australia. *Basin Res.* **18**, 189–203.

Meixner, A. J., Boucher, R. K., Yeates, A. N., Gunn, P. J., Richardson, L. M., and Frears, R. A., 1999. Interpretation of geophysical and geological data sets, Cooper Basin region, South Australia. Australian Geological Survey Organisation.

Merriman, R. J. and Frey, M., 1999. Patterns of very low-grade metamorphism in metapelitic rocks. In: Frey, M. and Robinson, D. Eds., *Low-grade metamorphism*. Blackwell Science, Cambridge.

Middleton, A. W., 2014. Geochemistry and geochronology of fluid flow events in high heat-producing granitic systems. PhD, University of Queensland.

Middleton, A. W., Uysal, I. T., Bryan, S. E., Hall, C. M., and Golding, S. D., 2014. Integrating $^{40}Ar–^{39}Ar$, $^{87}Rb–^{87}Sr$ and $^{147}Sm–^{143}Nd$ geochronology of authigenic illite to evaluate tectonic reactivation in an intraplate setting, central Australia. *Geochim. Cosmochim. Acta* **134**, 155–174.

Moore, D. M. and Reynolds, R. C. J., 1997. *X-ray Diffraction and the Identification and Analysis of Clay Minerals*. Oxford University Press, Oxford.

Müller, R. D., Dyksterhuis, S., and Rey, P., 2012. Australian paleo-stress fields and tectonic reactivation over the past 100 Ma. *Aust. J. Earth Sci.* **59**, 13–28.

O'Neil, J. R., Shaw, S. E., and Flood, R. H., 1977. Oxygen and Hydrogen Isotope Compositions as Indicators of Granite Genesis in the New England Batholith, Australia *Contrib. Mineral. Petr.* **62**, 313–328.

O'Sullivan, P. B., Kohn, B. P., Foster, D. A., and Gleadow, A. J. W., 1995. Fission track data from the Bathurst Batholith: evidence for rapid mid-Cretaceous uplift and erosion within the eastern highlands of Australia. *Aust. J. Earth Sci.* **42**, 597–607.

Parnell, J., Monson, B., and Tosswill, R. J., 1990. Petrography of thoriferous hydrocarbon nodules in sandstones and their significance for petroleim exploration. *J Geol Soc London* **147**.

Pearce, R. B., Clayton, T., and Kemp, A. E. S., 1991. Illitization and organic maturity in Silurian sediments form the southern Uplands of Scotland. *Clay Miner.* **26**, 199–210.

Perry, E. A. and Hower, J., 1970. Burial diagenesis in Gulf Coast peletic sediments. *Clays Clay Miner.* **18**, 165–177.

Pollastro, R. M., 1993. Considerations and applications of the illite/smectite geothermometer in hydrocarbon-bearing rocks of Miocene to Mississippian age. *Clays Clay Miner.* **41**, 119–133.

Polya, D. A., Foxford, K. A., Stuart, F., Boyce, A. J., and Fallick, A. E., 2000. Evolution and paragenetic context of low δD hydrothermal fluids from the Panasqueira W–Sn deposit, Portugal: New evidence from microthermometric, stable isotope, noble gas and halogen analyses of primary fluid inclusions. *Geochim. Cosmochim. Acta* **64**, 3357–3371.

Reeves, E. P., Seewald, J. S., and Sylva, S. P., 2012. Hydrogen isotope exchange between n-alkanes and water under hydrothermal conditions. *Geochim. Cosmochim. Acta* **77**, 582–599.

Reuter, A. and Dallmeyer, R., 1987. Significance of Ar^{40}/Ar^{39} age spectra of whole-rock and constituent grain-size fractions from anchizonal slates. *Chem. Geol.* **66**, 73–88.

Reynolds, R. C. J. and Hower, J., 1970. The nature of interlayering in mixed-layer illite-montmorillonites. *Clays Clay Miner.* **18**, 25–36.

Roberts, D. C., Carroll, P. G., and Sayers, J., 1990. The Kalladeina Formation - A Warburton Basin Cambrian carbonate play. *The APEA Journal* **30**, 166–184.

Rolland, Y., Cox, S. F., Boullier, A.-M., Pennacchioni, G., and Mancktelow, N., 2003. Rare earth and trace element mobility in mid-crustal shear zones: insights from the Mont Blanc Massif (Western Alps). *Earth Planet. Sci. Lett.* **214**, 203–219.

Rousset, D. and Clauer, N., 2003. Discrete clay diagenesis in a very low-permeable sequence constrained by an isotopic (K–Ar and Rb–Sr) study. *Contrib. Mineral. Petr.* **145**, 182–198.

Salvi, S. and William-Jones, A. E., 1990. The role of hydrothermal processes in the granite-hosted Zr, Y, REE deposit at Strange Lake, Quebec / Labrador: Evidence from fluid inclusions. *Geochim. Cosmochim. Acta* **54**.

Salvi, S. and William-Jones, A. E., 1996. The role of hydrothermal processes in concentrating high-field strength elements in the Strange Lake peralkaline complex, northeastern Canada. *Geochim. Cosmochim. Acta* **11**, 1917-1932.

Schimmelmann, A., Sessions, A. L., Boreham, C. J., Edwards, D. S., Logan, G. A., and Summons, R. E., 2004. D/H ratios in terrestrially sourced petroleum systems. *Organic Geochemistry* **35**, 1169–1195.

Schimmelmann, A., Sessions, A. L., and Mastalerz, M., 2006. Hydrogen Isotopic (D/H) Composition of Organic Matter During Diagenesis and Thermal Maturation. *Annual Review of Earth and Planetary Sciences* **34**, 501–533.

Sharp, Z. D., 1990. Laser-based microanalytical method for the in situ determination of oxygen isotope ratios of silicates and oxides. *Geochim. Cosmochim. Acta* **54**.

Sheppard, S. M. F., 1986. Characterization and isotopic variation in natural waters. In: Valley, J. W., Taylor, H. P. J., and O'Neil, J. R. Eds., *Stable isotopes in high temperature geological processes: Reviews in mineralogy*. Mineralogical Society of America.

Sheppard, S. M. F. and Gilg, H. A., 1996. Stable isotope geochemistry of clay minerals. *Clay Miner.* **31**, 1–24.

Simoneit, B. R. T., 1992. Organic matter alteration and fluid migration in hydrothermal systems. In: Parnell, J. (Ed.), *Geofluids: Origin, Migration and Evolution of Fluids in Sedimentary Basins*. Geological Society Special Publication, London.

Skirrow, R. S., Jaireth, S., Huston, D. L., Bastrakov, E. N., Scholfield, A., van der Wielen, S. E., and Barnicoat, A. C., 2009. Uranium mineral systems: Processes, exploration criteria and a new deposit framework. Geoscience Australia, **2009/20**.

Środoń, J., 2009. The charge of component layers of illite–smectite in bentonites and the nature of end-member illite. *Clays Clay Miner.* **57**, 649–671.

Stephens, C. J., 1991. The Mungore Cauldron and Gayndah Centre Late Triassic large-scale silicic volcanism in the New England Fold Belt near Gayndah, southeastern Queensland. PhD The University of Queensland.

Sun, X., 1997. Structural style of the Warburton Basin and control in the Cooper and Eromanga Basins, South Australia. *Exploration Geophysics* **28**, 333–339.

Sun, X., 1999. Fracture analysis of the Eastern Warburton Basin (Early Proterozoic), South Australia. Primary Industries and Resources, South Australia.

Taylor, H. P., Jr.,, 1997. Oxygen and hydrogen isotope relationships in hydrothermal mineral deposits. In: Barnes, H. L. (Ed.), *Geochemistry of hydrothermal ore deposits*. Wiley, New York.

Taylor, S. R. and McLennan, S. M., 1985. *The Continental Crust: Its Composition And Evolution*. Blackwell, Oxford.

Teichmüller, R. and Teichmüller, M., 1986. Relation between coalification and palaeogeothermics in Variscan and Alpidic foredeeps of western Europe. In: Buntebarth, G. and Stegena, L. Eds., *Palaeogeothermics*. Springer-Verlag, New York.

Thornton, R. C. N., 1979. Regional stratigraphic analysis of the Gidgealpa Group, southern Cooper Basin, Asutralia. *Australian Geological Survey Bulletin* **49**, 140–145.

Ting, F. T. C., 1978. Petrographic techniques in coal analysis. In: Karr, C. (Ed.), *Analytic Methods for Coal and Coal Products*. Academic Press, New York.

Truesdell, A. H. and Hulston, J. R., 1980. Isotopic evidence on environments of geothermal systems. In: Fritz, P. and Fontes, J. C. Eds., *Handbook of Environmental Isotope Geochemistry*. Elsevier, Amsterdam.

Uysal, I. T., 1999. Mineralogy and isotope geochemistry of authigenic clay and carbonate minerals in Late Permian coal measure, Bowen Basin, Queensland: Implications for thermal and fluid flow history. PhD, University of Queensland.

Uysal, I. T., Gasparon, M., Bolhar, R., Zhao, J.-X., Feng, Y.-X., and Jones, G., 2011a. Trace element composition of near-surface silica deposits - A powerful tool for detecting hydrothermal mineral and energy resources. *Chem. Geol.* **280**, 154–169.

Uysal, I. T., Glikson, M., Golding, S. D., and Audsley, F., 2000a. The thermal history of the Bowen Basin, Queensland, Australia: vitrinite reflectance and clay mineralogy of Late Permian coal measures. *Tectonophysics* **323**, 105–129.

Uysal, I. T., Glikson, M., Golding, S. D., and Southgate, P. N., 2004. Hydrothermal control on organic matter alteration and illite precipitation, Mt Isa Basin, Australia. *Geofluids* **4**, 131–142.

Uysal, I. T. and Golding, S. D., 2003. Rare earth element fractionation in authigenic illite-smectite from Late Permian clastic rocks, Bowen Basin, Australia: implications for

physico-chemical environments of fluid during illitization. *Chem. Geol.* **193**, 167–179.

Uysal, I. T., Golding, S. D., and Audsley, F., 2000b. Clay-mineral authigenesis in the late Permian Coal measures, Bowen Basin, Queensland, Australia. *Clays Clay Miner.* **48**, 351–365.

Uysal, I. T., Golding, S. D., and Baublys, K., 2000c. Stable isotope geochemistry of authigenic clay minerals from Late Permian coal measures, Queensland, Australia: implications for the evolution of the Bowen Basin. *Earth Planet. Sci. Lett.* **180**, 149-162.

Uysal, I. T., Golding, S. D., Bolhar, R., Zhao, J.-X., Feng, Y.-X., Baublys, K., and Greig, A., 2011b. CO_2 degassing and trapping during hydrothermal cycles related to Gondwana rifting in eastern Australia. *Geochim. Cosmochim. Acta* **75**, 5444–5466.

Uysal, I. T., Golding, S. D., and Thiede, D. S., 2001. K–Ar and Rb–Sr dating of authigenic illite–smectite in Late Permian coal measures, Queensland, Australia: implication for thermal history. *Chem. Geol.* **171**, 195–211.

Uysal, I. T., Mutlu, H., Altunel, E., Karabacak, V., and Golding, S. D., 2006. Clay mineralogical and isotopic (K-Ar, $\delta^{18}O$, δD) constraints on the evolution of the North Anatolian Fault Zone, Turkey. *Earth Planet. Sci. Lett.* **243**, 181-194.

Van Heeswijck, A., 2010. Late Paleozoic to Early Mesozoic deformation in the northeastern Galilee Basin, Australia. *Aust. J. Earth Sci.* **57**, 431–451.

Veevers, J. J., 1984. *Phanerozoic Earth History of Australia*. Clarendon Press, Oxford.

Veevers, J. J., 2004. Gondwanaland from 650–500 Ma assembly through 320 Ma merger in Pangea to 185–100 Ma breakup: supercontinental tectonics via stratigraphy and radiometric dating. *Earth Science Reviews* **68**, 1–132.

Veevers, J. J., Powell, C. M., and Roots, S. R., 1991. Review of seafloor spreading around Austrlia. 1. Synthesis of spreading. *Aust. J. Earth Sci.* **38**, 373–389.

Verdel, C., van de Pluijm, B. A., and Niemi, N., 2012. Variation of illite/muscovite $^{40}Ar/^{39}Ar$ spectra during progressive low-grade metamorphism: an example from the US Cordillera. *Contrib. Mineral. Petr.* **164**, 521–536.

Werner, D. and Doebl, F., 1974. Eine geothermische Karte des Rheingrabenuntergrundes. In: Illies, J. H. and Fuchs, K. Eds., *Approaches to Taphrogenesis*. Inter-Union Communications on Geodynamic Sienctific Reports.

William-Jones, A. E., Migdisov, A. A., and Samson, I. M., 2012. Hydrothermal mobilisation of the Rare Earth Elements – a Tale of "Ceria" and "Yttria". *Elements* **8**, 355–360.

Wilson, L., Wilson, M. J., Green, J., and Patey, I., 2014. The influence of clay mineralogy on formation damage in North Sea reservoir sandstones: A review with illustrative examples. *Earth Science Reviews* **134**, 70–80.

Wolf, M., 1988. Torf und Kohle. In: Füchtbauer, H. (Ed.), *Sedimente und Sedimentgesteine*. Schweizerbart, Stuttgart.

Wood, S. A., 1990. The aqueous geochemistry of the rare-earth elements and yttrium: 2. Theoretical predictions of speciation in hydrothermal solutions to 350°C at saturation water vapour pressure. *Chem. Geol.* **88**, 99–125.

Woolley, A. R., 1987. Lithospheric metasomatism and the petrogenesis of the Chilwa Province of alkaline igneous rocks and carbonatites, Malawi. *Journal of African Earth Sciences* **6**, 891–898.

Yardley, B. W. D., A., B. D., Bottrell, S. H., and Diamond, L. W., 1991. Post-metamorphic gold–quartz veins from N. W. Italy: the composition and origin of the ore fluid. *Mineral. Mag.* **57**, 407–422.

Yau, Y. C., Peacor, D., Essene, E. J., Lee, J. H., and Kuo, L. C., 1987. Hydrothermal treatment of smectite, illite, and basalt to 460°C: Comparison of natural with hydrothermally formed clay minerals. *Clays Clay Miner.* **35**, 241–250.

Yeh, H. W., 1980. D/H ratios and late-stage dehydration of shales during burial. *Geochim. Cosmochim. Acta* **44**, 341–352.

Ziegler, K., Sellwood, B. W., and Fallick, A. E., 1994. Radiogenic and stable isotope evidence for age and origin of authigenic illites in the Rotliegend, southern North Sea. *Clay Miner.* **29**, 555–565.

Zwingmann, H., Clauer, N., and Gaupp, R., 1999. Structure-related geochemical (REE) and isotopic (K–Ar, Rb–Sr, δ18O) characteristics of clay minerals from Rotliegend sandstone reservoirs (Permian, northern Germany). *Geochim. Cosmochim. Acta* **63**, 2805–2823.

Figure Captions

Figure 1.

(A) Location of the Warburton–Cooper–Eromanga Basin system in Australia. (B) Close-up view of sample area including locations of the Big Lake Suite granite plutons, drill-holes and the Gidgealpa (GR), Merrimelia (MR), Yanpurra (YR) and Innamincka (IR) ridge system.

Figure 2.

Depth versus illite crystallinity value . Samples show an irregular distribution with depth, an atypical characteristic of basin systems.

Figure 3.

Cross-polarised light photomicrograph of illite-rich alteration of Big Lake Suite granite replacing primary feldspars and micas (A), back-scatter electron (BSE) image of altered zircon (Zrn) intergrown with xenotime (Xtm) and thorite (Thr; B) and colloform Th-rich bastnaesite (Bas) intergrown with illite (Ill; C).

Figure 4.

BSE (A) and SE (B) photomicrographs of illite with lath-like and needle-like morphologies, respectively.

Figure 5.

Depth against VR estimated palaeotemperature for the Nappamerri Trough and Gidgealpa–Merrimelia–Innamincka Ridge

Figure 6.

Calculated δD and $\delta^{18}O$ fluid values in equilibrium with illite-rich clays from the Nappamerri Trough relative to Late Cretaceous meteoric water (cf. Uysal et al., 2011b). Scenario I models

a potential J-shaped evolution of meteoric waters. Whereas scenario II assumes a divergent trajectory to form two distinct populations, labelled as A and B, which comprise stratigraphically shallower samples with average δD values of –86‰ (Pop. A) and deeper samples with more negative δD values (average = –112‰; Pop. B).

Figure 7.

Depth against δD mineral (square) and calculated δD fluid (triangle) values in equilibrium with illite sampled from the Nappamerri Trough. Samples BL57_1748.94 and MB1_2816.5 were, however, excluded from the regression.

Figure 8.

Calculated δD fluid and $\delta^{18}O$ values in equilibrium with illite-rich clays from the GMI Ridge compared to that of formation waters for high and low latitude basins (Clayton et al., 1966). Meteoric waters may have undergone extensive oxygen isotopic exchange characteristic of open, geothermal systems.

Figure 9.

Upper continental crust-normalised (UCC) REE diagrams for unaltered and altered granite (A), ~86 Ma illites (B), ~94 Ma residue separates (C), ~94 Ma untreated–leachate separates (D) and UCC-normalised trace element diagram for selected leachate (Lch), residue (Res) and unaltered granite samples (E).

Figure 10.

Acid-leached residue separates from the Nappamerri Trough (~87 and ~100 Ma) exhibit positive correlations between calculated Zr/Hf, Gd/Lu and Th against δD fluid values (A – C) as well as estimated palaeotemperature and Y/Ho (D), and negative correlations between ΣREE and Th and calculated $\delta^{18}O$ fluid values (E & F; excluding sediment samples).

Figure 11.

Upper continental crust-normalised (UCC) REE diagrams for residue (A) and leachate separates (B) from the GMI Ridge.

Figure 12.

Acid-leached residue separates from the GMI ridge (~323 Ma) exhibit positive correlations when plotting calculated Y/Ho versus $\delta^{18}O$ fluid values ,and Gd/Lu versus ΣREE (A & B) but give inverse correlations for calculated δD fluid values versus La/Lu (C).

Figure 13.

Calculated $\delta^{18}O$ illite values of an altered granitic rock versus model water/rock ratios for an open system. Calculations assumed initial δ^{i}_{rock} $\delta^{18}O$ values of 10‰ (O'Neill et al., 1977) and δ^{i}_{water} $\delta^{18}O$ values of –12‰ (Uysal et al., 2011b). This plot shows that authigenic illite in environment A_{II} will have higher $\delta^{18}O$ values compared to those in A_I due to decreasing water/rock ratios. However, if illites precipitate under higher water/rock ratios (B_I) they will have more negative $\delta^{18}O$ values compared to A_I.

Table 1. Illite cystallinity values, vitrinite reflectance (VR) estimated palaeotemperatures and oxygen–hydrogen data for clays. Calculated $\delta^{18}O$ and δD values use VR estimated palaeotemperatures.

Sample	Grain	Illite crystallini	VR estimated palaeotemperat	Mineral	Mineral δD	Water	Water δD

	Size	ty value	ure	$\delta^{18}O$		$\delta^{18}O$	
Nappamerri Trough							
BL57 1748.94	<0.5	1.12	140	5.0	-101	-5.3	-78
BL1 3057.3	2-0.5	0.61	290	-1.8	-110	-5.6	-100
MB1 2816.5	2-0.5	0.70	275	8.5	-116	4.2	-105
MB1 2847.75	2-0.5	0.58	280	1.6	-98	-2.5	-87
MB1 2851.0	2-0.5	0.47	280	2.5	-99	-1.6	-88
MB1 2851.9	2-0.5	0.57	280	2.1	-102	-2.0	-91
MB1 2857.4 - A	2-0.5	0.57	280	2.7	-101	-1.4	-90
MB2 2717.5	<0.5	1.09	265	5.0	-86	0.5	-75
MB7 2453.5	2-0.5	0.56	225	9.7	-90	3.9	-76
McL1 3575.5	2-0.5	0.83	335	2.3	-119	-0.4	-112
McL1 3593.2	<0.5	0.59	335	2.6	-117	-0.1	-110
McL1 3749.1	2-0.5	0.38	350	1.7	-121	-0.6	-115
MB72 2999.6	<2	0.59	290	2.2	-96	-1.6	-86
MB72 3000.5	<2	0.57	290	1.9	-92	-1.9	-82
MB72 3003.2	<2	0.59	290	1.9	-98	-1.9	-88
MB72 3005	<2	0.58	290	2.2	-98	-1.6	-88
MB72 3008.6	<2	0.58	295	2.1	-100	-1.5	-90
MB_72 _ 3009.9	<1	0.56	295	1.2	-99	-2.4	-89
MB_72 _ 3011.1	1-2	0.58	295	1.5	-91	-2.1	-81

MB_72_3012	<1	0.56	295	1.8	-83	-1.8	-74
GMI Ridge							
T1 2933.9	2-0.5	0.55	170	7.8	-100	-0.6	-81
T7 3032.3	2-0.5	0.63	170	7.4	-92	-1.0	-73
T7 3032.3	<0.5	0.63	170	7.1	-78	-1.3	-59
T10 3005.2	2-0.5	0.68	170	7.1	-91	-1.3	-72
Mer2-2541.7	<2	0.61	160	11.0	-91	2.1	-71
Mer2-2617.35	<0.5	0.73	165	11.6	-88	3.0	-68
Mer2-2653.4	<0.5	0.74	165	11.8	-89	3.2	-70
Mer2-3895	<0.5	0.73	195	11.9	-94	4.7	-77
Mer1-3144.5	<2	0.83	175	10.7	-99	2.5	-80
Mer1-3039.5	2-1	0.95	170	11.7	-88	3.3	-69
Mer1-3039.5	1-0.5	-	170	10.6	-93	2.2	-73
Mer3-2589.2	1-0.5	0.56	160	9.5	-91	0.6	-71
Gil1-3843.5	1-0.5	0.61	195	8.7	-92	1.5	-75
W1 2936.0	2-0.5	0.55	170	9.6	-96	1.2	-77
W1 2936	<0.5	0.55	170	8.6	-95	0.2	-76

Table 2. Trace element data for whole-rock and illite from the Nappamerri Tough.

Sa	Cr	Al	Li	Be	Sc	V	Cr	Co	Ni	Rb	Sr	Y	Zr	Nb	Sn	Cs	Ba	La	Ce	Pr	Nd	Sm	Eu	Gd	Tb	Dy	Ho	Er	Tm	Yb	Lu	Hf	Ta	Pb	Th	U

mple_(Drillhole_depth)	ain Size	iquot	*Whole-rock sample*
			MB
			43.
			42.
			71.
			15.
			80.
			26.
			47.
			304
			21.
			93.
			353
			24.
			13.
			31.
			103
			114
			157
			22.
			70.
			13.
			0.06
			13.
			25.
			16.
			34.
			10.
			16.
			10.
			14.
			10.
			16.
			43.
			88.
			26.

1_28477.75			2	1	2	8	3	7	6		5	1		0	3	7				0	3	3	0	7	1	4	4	1	1	3	9	2	4	7	3	0
MB1_28577.4			54.5	5.42	7.89	17.3	6.50	3.52	3.93	287	24.9	110	362	24.0	13.2	34.4	100	135	199	26.0	83.5	16.2	0.74	16.5	2.99	19.1	40.4	11.9	1.90	12.2	1.79	10.2	1.56	5.71	82.4	23.6
MB1_28952.2			28.7	7.62	3.51	7.69	3.05	1.82	2.62	371	37.1	44.5	111	14.7	5.9	18.8	489	74.9	141	15.3	48.7	8.64	0.45	7.21	1.20	7.33	1.53	4.58	0.73	4.70	0.69	3.44	1.49	21.0	45.7	21.0
Clay Fractions																																				

MB72_30006.1	<2	U	173	5.52	2.44	3.82	27.6	2.65	3.11	333	37.5	13.5	10.5	5.09	22.4	56.2	193	2.33	4.60	0.52	1.80	0.66	0.04	1.26	0.27	1.82	0.42	1.25	0.20	1.22	0.17	0.32	0.54	179	9.38	2.21
MB72_30003.2	<2	U	280	7.77	7.06	9.73	54.7	4.38	5.04	721	41.9	21.5	110	10.7	17.3	122	423	6.09	24.6	1.88	8.78	3.23	0.15	2.70	0.45	3.14	0.79	2.86	0.58	4.62	1.08	2.94	1.40	188	25.2	15.6
MB72_30008.6	<2	U	348	7.19	4.81	7.28	51.7	4.89	4.76	705	40.9	14.8	25.0	9.8	108	117	507	1.93	8.02	0.36	1.37	0.57	0.03	1.13	0.28	2.08	0.49	1.56	0.27	1.81	0.27	0.80	1.14	155	13.5	5.01
MB72_30005	<2	U	233	8.65	4.51	8.90	38.6	4.98	4.00	728	30.5	10.2	28.4	34.4	8.66	115	260	3.68	11.7	0.59	1.86	0.60	0.03	0.95	0.23	1.64	0.39	1.28	0.23	1.53	0.22	1.06	3.53	316	17.8	10.6
M	<	U	3	6	4	1	4	2	3	6	3	2	4	8	1	1	3	1	6	0	1	0	0	1	0	3	0	3	0	4	0	1	1	8	1	6

B72_30000.5	2		15	.20	.42	1.1	4.5	.86	.72	67	5.9	8.3	7.5	.01	0.7	04	05	.92	.88	.42	.45	.61	.04	.61	.46	.70	.94	.26	.61	.44	.69	.38	.01	6.6	3.1	.24
MB72_29999.6	<2	U	192	10.2	10.2	15.6	57.4	1.71	3.41	663	22.1	277	82.1	15.4	15.9	121	211	53.0	32.8	14.0	44.6	10.3	0.62	19.6	4.51	32.5	7.94	25.28	4.22	27.4	4.09	2.17	4.02	60.8	30.6	19.6
MB72_30008	<1	U	278	10.2	5.00	7.68	51.3	4.59	4.91	803	68.6	23.4	18.2	19.5	69.0	108	340	10.2	22.6	2.05	5.95	1.52	0.09	2.57	0.59	3.83	0.83	2.41	0.38	2.29	0.31	0.71	2.25	220	20.6	5.67
MB72_30008	<1	R	8.95	3.88	4.02	7.36	15.0	0.54	0.56	812	3.20	23.5	14.4	22.4	4.06	74.5	138	13.8	25.1	2.48	6.67	1.45	0.10	2.50	0.59	3.79	0.81	2.29	0.35	2.09	0.28	0.55	2.53	10.1	22.1	6.04
MB72	2–1	U	35.9	9.62	5.95	9.56	53.4	3.39	3.93	844	57.0	41.1	17.8	33.3	22.3	67.1	269	59.6	100	9.8	24.4	3.75	0.20	4.86	1.08	6.92	1.48	4.21	0.64	3.76	0.48	0.68	3.53	194	29.9	13.5

_3008																																				
MB72_3008	2_1	R	14.8	4.72	5.52	10.0	30.1	0.51	0.61	804	6.74	38.8	16.2	39.1	6.93	47.7	157	58.6	111	10.0	24.9	3.65	0.20	4.56	1.03	6.57	1.39	3.90	0.59	3.38	0.43	0.62	4.12	8.59	33.3	14.6
MB72_3009.9	2_1	U	43.4	14.0	6.64	9.46	67.0	4.63	5.54	1087	74.0	53.0	18.8	26.2	149	87.1	306	101	161	18.2	51.6	7.23	0.27	7.24	1.47	9.30	1.91	5.31	0.82	4.86	0.64	0.77	3.89	108	56.9	15.3
MB72_3009.9	<1	U	279	13.7	4.13	6.36	44.2	4.18	4.76	706	60.3	9.26	11.9	10.8	121	111	238	5.07	10.0	1.37	4.71	1.23	0.05	1.60	0.33	2.10	0.43	1.25	0.20	1.24	0.17	0.52	1.92	88.7	16.0	3.39
MB72	<1	L	7680	201	16.8	14.1	660	103	100	1018	2011	52.3	18.0	0.84	218	422	4502	16.4	42.4	7.36	34.7	13.8	0.50	12.6	1.91	10.6	2.05	5.96	1.00	6.53	0.90	0.63	0.01	262	23.8	7.02

_3009.9																																				
MB72_3009.9	<1	R	14.0	6.30	4.22	5.85	21.3	1.52	1.84	798	2.28	13.0	11.0	10.0	93.7	101	155	10.1	16.7	1.99	5.97	1.21	0.06	1.73	0.37	2.33	0.48	1.34	0.21	1.31	0.18	0.48	1.73	4.97	19.7	3.49
MB72_3011.1	2–1	U	69.1	13.8	7.63	11.2	118	2.58	5.08	1042	58.7	94.8	30.1	25.0	116	80.3	350	221	241	43.0	118	14.85	0.48	12.8	2.68	17.9	3.67	10.17	1.55	9.27	1.16	1.02	2.78	151	70.5	10.9
MB72_3011.1	2–1	L	815	120	20.6	22.7	776	33.4	66.4	642	994	40.1	37.1	0.91	276	376	365.6	18.5	45.2	8.73	41.0	14.8	0.49	11.5	1.62	8.76	1.72	4.89	0.84	5.68	0.79	0.95	0.02	3048	19.4	4.00
MB	2–	R	30	7.	5.	9.	77	1.	2.	89	13	82	25	23	98	56	17	19	21	38	10	12	0.	11	2.	15	3.	8.	1.	8.	1.	0.	2.	10	62	9.

72_30111.1	1		.2	15	99	19	.76	00	21	0	.3	.8	.1	.5	.8	.5	0	7	5	.2	4	.81	42	.0	34	.6	20	86	38	06	02	86	78	.8	.2	6
MB72_30111.1	<1	U	330	13.1	5.21	6.51	50.42	2.81	5.14	836	55.0	33.2	13.4	9.6	138	110	414	14.9	18.4	3.37	10.6	2.50	0.11	4.01	0.90	6.13	1.28	3.58	0.56	3.34	0.42	0.48	0.38	154	17.4	2.50
MB72_30111.1	<1	L	6005	164	23.0	14.8	769	51.2	77.8	1320	1099	67.4	41.1	1.66	196	541	5701	24.5	52.6	10.3	45.1	16.4	0.61	14.5	2.38	14.2	2.85	8.14	1.34	8.55	1.14	1.05	0.01	3111	29.8	5.67
MB72_30111.1	<1	R	15.2	4.93	3.98	5.52	13.80	0.45	1.24	744	2.14	29.5	11.0	11.4	113	81.0	14.4	13.6	15.8	2.86	8.35	1.77	0.09	3.24	0.77	5.44	1.13	3.14	0.48	2.89	0.36	0.40	1.20	4.13	15.6	2.15
M	<	U	2	1	5	8	6	4	6	7	5	1	2	1	1	1	4	4	1	1	4	1	0	2	0	2	0	1	0	1	0	1	2	1	4	7

B72_3012	2		84	6.0	.05	.53	1.4	.36	.14	47	1.5	4.1	7.3	9.8	07	30	11	.72	3.0	.30	.52	.43	.08	.04	.42	.64	.57	.71	.28	.87	.27	.00	.35	70	2.3	.12
MB72_3012	2–1	U	40.4	9.85	4.83	7.41	50.9	2.25	3.78	678	36.3	30.4	19.4	22.8	88.4	56.2	236	43.7	98.6	8.13	22.8	3.84	0.19	4.24	0.86	5.40	1.11	3.18	0.50	2.93	0.40	0.74	1.75	114	59.2	14.7
MB72_3012	2–1	L	791	140	15.2	16.8	604	49.5	74.3	718	121.9	31.1	11.7	1.34	350	411	4385	19.9	68.6	9.67	43.5	13.0	0.53	9.74	1.30	6.81	1.30	3.78	0.65	4.27	0.62	0.36	0.07	3735	25.3	6.23
MB72_3012	2–1	R	30.1	8.99	6.72	10.7	55.5	1.47	2.68	1008	7.38	44.4	29.2	38.6	105	69.6	191	63.6	142	11.6	31.9	5.21	0.26	5.95	1.23	7.73	1.59	4.59	0.71	4.24	0.58	1.09	4.54	14.7	88.0	21.5
McL1_359	2–0.5	U	13462	42.5	21.2	102	54.5	13.3	18.4	474	69.8	22.1	355	3.92	289	118	3451	19.1	83.4	4.29	15.0	3.07	0.67	3.25	0.60	4.07	0.93	2.85	0.49	3.36	0.50	6.48	0.32	49.6	19.3	5.47

3.2																																				
McL1_35933.2	2–0.5	L	382	63.4	4.56	11.5	9.5	245	119	200	1903	7.01	2.67	0.34	5.30	420	81995	6.07	10.8	1.30	4.87	1.31	-3.47	1.29	0.24	1.39	0.26	0.69	0.10	0.60	0.08	0.10	0.00	2092	1.45	1.11
McL1_35933.2	2–0.5	R	2784	7.41	16.0	79.2	44.2	4.91	12.9	385	17.7	18.8	207	3.59	299	81.3	498	7.87	47.5	1.71	5.88	1.28	0.39	1.83	0.45	3.39	0.80	2.53	0.45	3.04	0.45	5.01	0.29	8.53	18.1	4.39
McL1_35933.2	<0.5	U	460	3.19	6.66	48.4	25.0	12.4	15.2	352	81.3	13.8	118	0.59	8.10	193	3178	7.83	15.2	1.71	6.13	1.25	0.38	0.37	1.55	2.73	13.8	0.61	1.87	0.31	2.11	0.32	3.28	2.18	5.29	2.70
McL1_35	<0.5	R	552	1.96	8.75	65.4	34.3	5.19	11.8	480	11.1	18.9	164	0.86	6.09	229	777	10.9	21.8	2.45	8.69	1.75	0.53	0.52	2.18	3.76	18.9	0.84	2.59	0.43	2.92	0.44	4.60	3.07	7.42	3.81

93.2																																				
McL1_3749.1	2–0.5	U	19.2	18.6	4.73	13.7	8.89	6.80	10.6	991	94.1	8.32	6.31	6.93	1307	119	2206	39.4	82.6	8.98	28.5	4.10	0.11	1.58	0.25	1.50	0.32	0.92	0.14	0.90	0.12	0.27	1.16	34.0	12.9	1.96
McL1_3749.1	2–0.5	L	43.3	113	2.37	2.71	70.9	69.9	90.6	288	1903	8.76	1.81	3.57	24	358	53823	2.63	5.12	0.68	3.48	2.92	-2.30	2.70	0.38	1.92	0.34	0.92	0.14	0.90	0.13	0.09	0.04	609	2.54	1.58
McL1_3749.1	2–0.5	R	17.7	13.6	4.91	14.3	11.8	4.15	10.1	1397	13.8	8.17	6.74	7.30	345	110	524	40.3	89.3	9.31	29.1	4.09	0.15	1.48	0.24	1.44	0.29	0.88	0.14	0.85	0.11	0.29	1.19	5.90	13.4	2.03
McL1_3	<0.5	U	17.9	17.9	4.41	13.5	5.78	6.70	9.53	962	90.2	6.57	2.07	6.90	20	111	2055	11.6	25.2	2.81	9.21	1.65	0.11	0.20	1.11	1.20	6.57	0.24	0.70	0.11	0.66	0.09	0.13	3.81	9.06	1.70

749.1																																				
McL1_37749.1	<0.5	R	11.8	9.6	3.33	10.3	4.26	2.34	4.35	736	8.10	5.18	1.89	5.24	14	66.0	335	20.4	44.3	4.89	15.7	2.30	0.11	0.17	0.98	0.95	5.18	0.19	0.55	0.09	0.52	0.07	0.11	2.96	8.28	1.27
MB1_28577.4	2–0.5	U	8.77	4.44	4.32	18.4	16.05	2.35	3.05	822	37.2	36.7	11.3	20.9	1622	77.3	231	128	145	16.6	45.0	7.53	0.30	6.76	1.11	6.56	1.33	3.64	0.54	3.16	0.43	0.46	2.34	7.21	45.2	12.7
MB1_28577.4	2–0.5	L	28.9	19.6	2.22	1.39	69.5	9.92	23.7	103	330	16.7	0.83	0.93	5.38	165	1210	41.7	76.0	10.3	35.6	7.45	0.26	6.25	0.80	3.50	0.63	1.72	0.30	2.07	0.31	0.04	0.01	22.1	8.98	1.73
MB1_285	2–0.5	R	6.47	3.05	4.42	19.2	16.5	1.57	2.53	836	8.66	35.8	11.0	20.6	491	63.6	132	122	132	15.1	40.5	6.73	0.27	6.15	1.04	6.30	1.31	3.58	0.53	3.04	0.41	0.47	2.36	4.21	44.6	12.6

7.4																																						
MB1_28577.4	<0.5	U	29.22	55.85	39.95	17.11	23.84	2.84	2.89	769	50.3	16.18	20.24	39.97	478	128	295	10.2	15.10	1.81	5.67	1.28	0.06	1.79	0.39	2.68	0.60	1.76	0.29	1.91	0.28	0.84	0.43	4.46	15.2	3.14
MB1_28577.4	<0.5	L	486	56.1	4.91	2.14	245	26.2	84.7	133	897	31.2	1.90	1.99	97.7	176	339.6	44.2	81.8	10.6	36.8	8.27	0.24	8.26	1.25	6.15	1.13	3.17	0.55	3.70	0.54	0.13	0.00	32.7	1.11	1.92
MB1_28577.4	<0.5	R	6.87	3.40	3.94	17.6	21.9	1.70	2.66	778	3.18	16.5	22.1	4.14	955	126	135	8.86	1.2	1.45	4.38	0.97	0.05	1.53	0.36	2.61	0.60	1.78	0.29	1.87	0.28	0.90	0.47	3.52	16.0	3.28
MB1_28477.7	<0.5	U	60.9	5.44	7.89	20.6	20.8	5.86	6.02	734	66.0	14.2	22.5	7.65	548	182	391	15.3	18.3	2.87	8.98	1.72	0.07	1.83	0.37	2.52	0.58	1.85	0.35	2.59	0.41	1.01	0.77	4.39	38.0	7.52

5																																				
MB1_284475	<0.5	L	876	520	95.5	1.78	749	542	525	139	1.14	43.4	34.3	2.21	1.47	227	4906	370.1	520	8.97	29.9	6.55	0.15	7.21	1.38	8.50	1.78	5.33	0.98	6.86	0.98	0.28	0.00	29.9	13.4	34.1
MB1_284475	<0.5	R	16.6	2.887	7.88	21.8	20.8	30.2	6.16	752	3.24	12.0	23.1	7.87	324	223	129	13.3	15.5	2.40	7.40	1.39	0.06	1.45	0.30	2.09	0.49	1.60	0.30	2.28	0.37	1.03	0.80	2.48	38.8	7.66
MB1_284475	2–0.5	U	19.5	4.68	8.79	23.2	15.6	4.40	4.25	582	57.4	23.3	15.0	25.7	23.0	86.9	299	113	104	12.6	33.2	5.11	0.22	0.75	4.40	4.51	23.3	0.94	2.79	0.47	3.16	0.47	0.71	2.54	77.6	18.5
MB1_284475	2–0.5	R	13.6	2.36	8.63	24.3	14.7	2.30	4.01	589	7.24	20.0	15.2	24.8	21.1	64.7	157	97.7	89.5	10.1	25.6	3.73	0.18	0.63	3.37	3.89	20.0	0.82	2.49	0.42	2.84	0.41	0.71	2.83	73.6	17.7

75																																			
MB1_28511	2–0.5	U	10.0	3.78	5.57	16.4	19.6	7.24	5.18	736	49.3	16.4	10.8	14.7	1164	69.6	257	64.8	65.0	9.29	27.1	4.57	0.18	3.76	0.55	3.16	0.63	1.85	0.30	1.95	0.28	0.47	1.40	5.49	3.38	10.6
MB1_28511	2–0.5	L	3.07	1.53	0.08	0.09	2.29	2.72	1.02	7.25	45.7	1.28	0.15	0.02	4.09	14.1	141	2.10	3.07	0.50	1.69	0.34	0.01	0.32	0.05	0.27	0.05	0.14	0.02	0.17	0.02	0.00	0.00	2.77	0.38	0.12
MB1_28511	2–0.5	R	7.95	2.61	6.23	18.7	19.1	5.12	5.52	632	5.92	1.22	13.2	18.4	253	62.5	132	7.70	7.67	10.9	31.8	5.33	0.22	4.26	0.62	3.40	0.69	2.03	0.32	2.07	0.30	0.57	1.70	3.77	41.8	13.5
MB1_28511	2–0.5	U	15.1	6.03	8.92	26.3	27.3	11.3	7.30	859	84.5	26.8	16.9	24.7	27.9	106	403	100	102	15.1	44.6	7.60	0.31	0.94	6.23	5.19	26.8	1.04	3.00	0.49	3.23	0.47	0.79	2.95	52.8	17.8
MB1_28511	2–0.5	R	5.45	2.03	4.89	15.4	12.9	2.96	2.70	490	3.41	1.48	9.91	15.5	1.45	41.4	101	58.6	58.3	8.46	2.48	4.10	0.18	0.52	3.42	2.87	1.48	0.57	1.68	0.27	1.75	0.26	0.46	2.01	31.9	11.1
M	2	U	4	5	4	1	2	2	3	5	5	9	3	4	1	1	2	8	9	1	4	0	0	0	1	1	9	0	1	0	2	0	1	2	2	5

B1_28551.92	–0.5		0.0	.55	.96	6.9	6.8	.89	.79	41	6.4	.8	0.9	.28	9.6	32	91	.00	.36	.48	.71	.99	.05	.26	.18	.74	.78	.40	.36	.27	.13	.36	.29	.34	9	.15
MB1_28551.92	2–0.5	R	14.2	5.58	10.5	35.8	26.5	2.28	3.60	1124	12.6	25.8	26.6	40.0	35.8	97.7	208	180	152	21.7	57.7	8.77	0.37	1.05	7.02	5.50	25.8	1.05	2.97	0.49	3.21	0.47	1.16	4.96	93.5	25.8
MB1_28557.4	2–0.5	U	6.44	3.85	3.56	15.5	11.5	1.91	1.81	490	32.1	30.1	8.86	16.9	17.2	60.0	186	97.7	109	13.1	36.5	6.24	0.25	0.94	5.55	5.42	30.1	1.09	3.01	0.45	2.66	0.37	0.39	2.09	36.0	10.3
MB1_28557.4	2–0.5	R	3.93	2.36	3.57	15.1	9.5	1.13	1.18	485	8.13	32.0	8.49	17.2	15.5	41.8	115	108	114	13.8	37.4	6.20	0.26	0.98	5.68	5.73	32.0	1.16	3.20	0.46	2.76	0.37	0.37	2.05	39.4	10.2
MB	<1	U	58	10	9	89	10	5.	20	11	88	0.	31	2.	17	51	13	0.	0.	0.	0.	0.	0.	0.	0.	0.	0.	0.	0.	0.	0.	0.	0.	3.	0.	0.

2_2715.5			.7	.0		.1	6	31	.7	5	.8	49	.0	29	6	.0	58	19	55	07	32	10	00	11	02	16	04	12	02	19	03	90	19	16	87	82
MB2_2715.5	<1	L	26.4	6.05	2.87	4.64	11.7	1.41	4.05	7.13	130	0.53	0.16	0.01	1.24	1.27	468	0.42	0.94	0.12	0.50	0.14	0.05	0.17	0.02	0.12	0.02	0.06	0.01	0.05	0.01	0.01	0.00	3.25	0.51	0.12
MB2_2715.5	<1	R	38.5	5.19	9.6	90.6	108	4.77	20.1	442	14.7	3.24	36.2	2.57	74.4	86.2	85.8	5.74	11.3	1.26	4.32	0.75	0.12	0.58	0.09	0.54	0.12	0.38	0.06	0.47	0.08	1.09	0.23	2.28	3.56	0.91
MB2_2715.5	<0.5	U	120	12.9	11.6	90.6	110	11.4	39.3	436	178	8.25	27.6	1.98	10.7	140	1663	11	21	2.48	9.04	1.72	0.29	0.25	1.57	1.47	8.25	0.30	0.87	0.13	0.84	0.12	0.95	2.47	6.65	1.11
MB2_2	<0.5	R	44.8	5.07	9.7	83.3	97.3	8.20	30.4	370	48.1	6.64	23.6	2.23	5.35	110	690	9.02	18.0	2.06	7.43	1.38	0.21	0.20	1.22	1.19	6.64	0.25	0.71	0.11	0.70	0.10	0.80	2.18	4.26	1.04

715.5																																						
MB7_24533.4	<2	U	31.3	5.91	18.11	169	126	242.2	417	441	87.2	28.6	146	25.2	1136	183.3	766	780	237	17.3	59.9	10.5	1.79	8.01	1.09	5.84	1.16	3.31	0.51	3.27	0.47	4.62	2.37	44.3	26.8	7.48	
MB7_24533.4	<2	L	13.5	1.04	0.25	0.85	3.14	16.9	22.2	2.44	4.43	0.22	0.21	0.01	1.97	0.22	1.60	0.26	0.53	0.06	0.22	0.04	0.00	0.04	0.01	0.06	0.01	0.03	0.00	0.02	0.00	0.01	0.00	28.6	0.13	0.15	
MB7_24533.4	<2	R	17.7	4.93	20.0	174	132	79.0	21.9	382	97.2	32.4	156	26.5	161	19.1	673	880	178	19.5	67.3	11.8	2.02	8.86	1.22	6.42	1.26	3.67	0.55	3.60	0.52	4.92	2.42	15.8	29.8	8.04	
MB7_2453	2–0.5	U	47.5	18.0	57.6	504	362	518	99.2	970	188	66.1	326	62.3	493	490	1958	148	290	32.9	115	20.0	3.56	2.39	1.59	1.33	6.61	2.66	7.50	1.19	7.76	1.14	10.60	7.31	52.0	17.9	

.4																																					
MB7_24533.4	2–05	R	14.2	58.82	201	187	144	108	262	383	624	301	167	138	180	228	539	539	105	119	417	720	128	097	598	586	301	125	365	059	391	057	574	322	197	832
BL57_17488.94	2–05	U	158	331	97	115	786	151	328	236	401	180	117	657	110	337	534	250	494	373	127	209	311	119	512	103	279	034	195	028	344	492	78	615	510	
BL57_17488.94	2–05	L	058	061	012	043	103	103	970	407	132	158	018	001	809	036	200	036	087	011	052	025	073	053	009	048	110	024	003	017	002	001	000	611	147	038
BL57_17488.94	2–05	R	178	316	110	118	910	700	308	262	332	196	132	179	226	344	411	205	426	44	149	248	348	141	129	570	109	305	037	207	030	389	010	306	765	585
BL57_17	2–05	R	178	316	110	118	910	700	308	262	332	196	132	179	226	344	411	205	426	44	149	248	348	141	129	570	109	305	037	207	030	389	010	306	765	585

48.94																																				
BL57_1748.94	<0.5	U	11.1	2.19	4.79	69.0	51.7	16.4	29.7	221	228	5.17	38.0	14.0	9.5	2.67	420	24.5	49.9	4.78	16.1	2.62	0.44	0.25	1.91	1.35	5.17	0.28	0.75	0.10	0.61	0.09	1.20	1.32	11.5	1.43
BL57_1748.94	<0.5	R	3.42	0.89	2.62	43.5	33.1	2.65	11.2	131	24.5	2.51	24.0	8.72	3.07	1.54	98.5	16.8	32.2	3.27	10.8	1.67	0.27	0.13	1.10	0.65	2.51	0.14	0.37	0.05	0.31	0.04	0.76	0.81	7.05	0.77
BL1_3057.3	2–0.5	U	23.6	21.1	1.32	4.10	2.90	1.73	3.19	1255	38.8	9.11	1.97	6.55	19.2	149	167	8.65	18	2.04	6.74	1.54	0.02	0.23	1.31	1.35	9.11	0.28	0.86	0.15	1.08	0.16	0.12	8.21	6.06	1.80
BL1_	2–0.	R	16.5	16.8	1.40	4.80	2.96	1.29	2.87	1511	4.83	4.49	1.98	7.85	20.1	161	160	3.37	6.60	0.66	1.97	0.39	0.01	0.11	0.46	0.76	4.49	0.17	0.54	0.09	0.59	0.08	0.12	10.5	5.01	1.93

3057.3	5																																			
BL1_3057.3	<0.5	U	229	23.8	1.93	4.62	7.53	1.74	3.19	1967	64.7	27.6	7.21	11.5	367	268	153	24.6	57.9	5.48	17.3	3.83	0.05	3.54	0.66	4.23	0.92	2.82	0.50	3.25	0.46	0.30	3.00	25.7	24.6	6.75
BL1_3057.3	<0.5	L	224	8	0.71	0.28	2.74	0.66	0.98	130	86.6	8.65	0.43	0.53	3.25	45.3	24.5	13.7	30.0	3.33	10.9	2.52	0.03	1.94	0.27	1.35	0.25	0.76	0.14	1.03	0.16	0.02	0.00	22.3	5.82	0.67
BL1_3057.3	<0.5	R	21.2	19.0	1.95	5.60	6.74	1.46	3.56	1925	8.10	24.5	8.23	14.3	223	191	177	17.3	34.4	3.37	9.9	1.98	0.03	2.31	0.53	3.75	0.86	2.70	0.45	2.86	0.39	0.36	3.68	7.79	26	8.11

U = untreated, L = leachate, R = residue.

Table 3. Trace element data for illite from the GMI Ridge.

S	C	A	L	B	S	V	C	C	N	R	S	Y	Z	N	S	C	B	L	C	P	N	S	E	C	T	D	H	E	T	Y	L	H	T	P	T	U

sample_(Drillhole_depth)	rainSize	liquot	ieccrroibrrrbnsaaaerddnnudbyorrmbufabh	
Mer1_30395	<0.5	U	45.7 40.9 10.9 96.6 71.9 10.9 26.2 28.1 11.9 13.2 36.8 20.50 15.2 16.3 14.17 14.8 31.2 3.65 14.1 3.38 0.68 0.47 3.22 2.58 0.51 1.44 0.22 1.43 0.21 1.12 0.22 6.29 7.38 2.73	
Mer1_303	<0.5	L	49.3 1.90 2.71 4.60 8.07 1.79 1.81 7.56 1.09 6.41 0.87 0.01 2.30 0.23 8.51 1.35 5.25 0.94 5.37 2.28 0.54 0.36 2.68 1.67 0.27 0.59 0.06 0.34 0.04 0.06 0.00 4.18 3.44 0.53	

9.5																																				
Mer1_30399.5	<0.5	R	90.01	40.00	14.16	152	107	155	40.1	458	421	129	582	405	109	263	114.0	224	448	44.74	159	250	04.41	03.11	1.80	2.002	0.048	1.55	0.27	1.84	0.29	1.71	0.38	45.2	74.8	3.78
Mer1_31444.5	<0.5	U	77.8	6.56	15.4	92.6	100	10.2	26.3	33.3	99.2	16.1	66.2	7.17	204	23.1	120.7	35.0	68.8	7.41	25.6	4.48	0.81	0.51	3.44	2.92	0.62	1.88	0.30	2.05	0.31	1.89	0.58	28.9	18.2	3.43
Mer1_31444.5	<0.5	L	59.8	1.54	0.83	1.62	0.92	0.27	1.15	5.51	48.6	3.97	0.30	0.01	1.03	0.23	5.56	1.19	3.90	0.70	3.71	1.40	0.32	0.21	1.51	1.00	0.17	0.38	0.04	0.23	0.03	0.02	0.00	6.57	3.58	0.317
Mer1_31	<0.5	R	12.0	5.32	17.2	107	115	11.6	29.8	400	51.2	13.6	78.6	8.72	168	27.7	5.56	39.8	76.8	7.85	25.3	3.40	0.54	0.33	2.00	2.11	0.51	1.72	0.30	2.12	0.33	2.21	0.71	24.4	16.6	3.67

44.5																																				
Mer2_2541.7	<0.5	U	21.6	7.51	18.5	101	128	7.85	34.6	352	183	15.9	83.9	7.05	117	23.3	2351	30.2	59.7	6.41	21.8	3.63	0.56	0.39	2.56	2.49	0.58	1.93	0.33	2.25	0.35	2.32	0.59	32.2	16.6	3.70
Mer2_2541.7	<0.5	L	17.9	3.89	2.43	7.04	13.9	0.52	2.00	10.1	105	1.68	0.81	0.01	1.30	0.22	2246	0.64	1.66	0.25	1.20	0.41	0.02	0.08	0.54	0.41	0.07	0.16	0.02	0.10	0.01	0.08	0.00	13.3	2.37	0.70
Mer2_2541.7	<0.5	R	8.20	5.22	19.7	10.9	136	8.66	38.5	397	115	16.8	95.2	8.03	81.2	26.6	601	34.0	67.5	7.16	23.7	3.80	0.65	0.37	2.47	2.45	0.61	2.08	0.36	2.51	0.39	2.59	0.67	24.9	17.0	3.61
Mer2_2	<0.5	U	18.4	7.75	15.5	94.8	127	8.94	37.6	373	185	22.9	13.3	4.30	151	18.8	1490	27.2	54.2	5.94	20.9	3.72	0.67	0.50	2.89	3.47	0.83	2.59	0.41	2.69	0.40	3.85	0.51	12.4	15.7	6.26

617.35																																				
Mer2_26617.35	<0.5	L	14.9	3.75	0.65	4.54	9.80	0.37	1.22	6.24	121	1.90	0.94	0.00	1.64	0.14	1255	0.61	1.79	0.29	1.44	0.51	0.08	0.10	0.68	0.47	0.08	0.17	0.02	0.10	0.01	0.09	0.00	3.23	0.44	0.30
Mer2_26617.35	<0.5	R	6.38	5.22	16.3	96.8	127	9.17	38.3	391	84.8	22.6	142	4.69	82.9	19.9	44.9	28.6	56.8	6.15	21.2	3.55	0.65	0.46	0.52	0.30	0.81	0.61	0.42	0.76	0.42	4.04	0.42	10.3	16.5	6.40
Mer2_26653.4	<0.5	U	13.8	3.79	13.0	89.4	140	11.1	23.6	243	133	34.0	66.9	7.19	129	13.2	1295	42.3	94.0	11.4	46.3	12.0	2.65	1.61	11.8	7.89	1.39	3.41	0.44	2.68	0.38	1.91	0.61	10.3	18.5	4.37
Me	<0	L	15	4.	0.	7.	10	0.	1.	10	13	1.	0.	0.	1.	0.	13	0.	1.	0.	0.	0.	0.	0.	0.	0.	0.	0.	0.	0.	0.	0.	0.	6.	0.	0.

r2_26533.4	.5		.9	34	89	23	.2	59	60	.7	1	36	84	00	17	21	36	52	32	19	90	29	02	06	36	31	06	13	02	09	01	08	00	18	45	39
Mer2_26533.4	<0.5	R	9.62	6.41	22.8	102	182	8.82	33.0	451	162	32.1	23.4	9.75	105	26.1	566	55.6	103	11.3	37.8	5.59	0.94	0.59	3.29	4.41	1.13	3.85	0.67	4.53	0.70	6.66	0.87	13.9	22.3	4.64
Mer2_38955	<0.5	U	55.5	13.8	20.3	115	171	10.3	26.9	360	241	13.5	48.0	6.36	237	19.0	1148	48.2	95.6	9.71	31.9	4.95	0.79	0.47	3.35	2.59	0.53	1.61	0.26	1.80	0.28	1.47	0.59	14.8	17.9	4.09
Mer2_38955	<0.5	L	47.3	8.17	3.09	7.74	16.0	1.15	3.24	6.74	207	5.56	1.46	0.01	0.86	0.14	727	2.19	7.13	1.05	5.28	1.71	0.32	0.25	1.70	1.27	0.24	0.60	0.08	0.47	0.06	0.09	0.00	8.91	4.67	1.00
Mer2_	<0.5	R	12.0	7.05	19.0	110	159	9.67	24.1	377	42.0	8.86	48.1	6.67	185	19.9	499	49.3	95.5	9.32	28.5	3.59	0.52	0.27	1.94	1.52	0.34	1.14	0.20	1.45	0.24	1.43	0.60	6.61	14.6	3.41

3895																																						
Mer3_25889.2	<0.5	U	38.6	7.52	19.3	167	180	350.3	47.3	358	311	484.4	246	90.03	300	110.0	1483	86.7	177	19.5	70.1	13.9	3.26	19.6	12.6	10.5	1.97	5.44	0.82	5.31	0.78	6.89	0.86	108.6	23.1	8.59	
Mer3_25889.2	<0.5	L	24.2	2.68	0.32	1.55	25.56	26.67	31.3	4.71	2.20	0.39	0.35	0.01	3.45	0.25	1.97	0.67	1.37	0.17	0.163	0.13	0.02	0.02	0.12	0.09	0.02	0.04	0.01	0.04	0.00	0.02	0.00	94.7	0.21	0.15	
Mer3_25889.2	<0.5	R	18.1	6.00	2.07	1.84	17.3	11.7	19.6	3.95	3.17	52.5	2.78	1.06	1.58	1.21	1.458	94.5	1.94	2.13	7.60	1.50	3.56	2.13	1.38	1.14	2.16	5.93	0.90	5.83	0.86	7.83	1.01	24.0	25.3	9.46	
Gil1_3	<0.5	U	71.2	8.01	7.91	1.11	1.44	2.99	6.57	2.73	2.40	9.70	2.89	5.24	3.71	4.01	6.83	1.33	2.80	3.42	1.35	3.04	0.51	0.37	2.51	1.95	0.37	1.00	0.14	0.88	0.13	0.93	0.48	24.7	1.13	3.97	

843.5																																				
Gil1_3843.5	<0.5	R	18.5	6.03	8.68	143	173	6.33	40.7	361	25.8	4.09	37.6	7.24	348	54.5	673	14.4	25.9	2.59	7.55	0.77	0.10	0.09	0.48	0.63	0.15	0.54	0.10	0.65	0.10	1.18	0.66	5.73	8.01	3.94

U = untreated, L = leachate, R = residue.

Figure 1

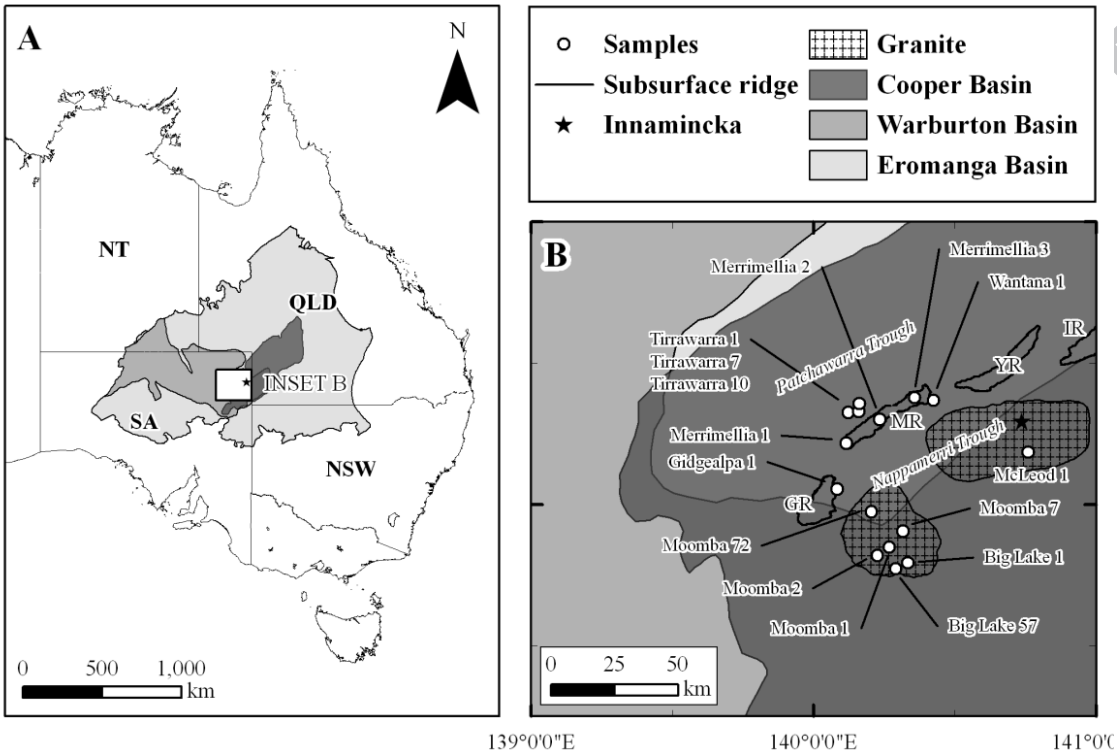

Figure 2

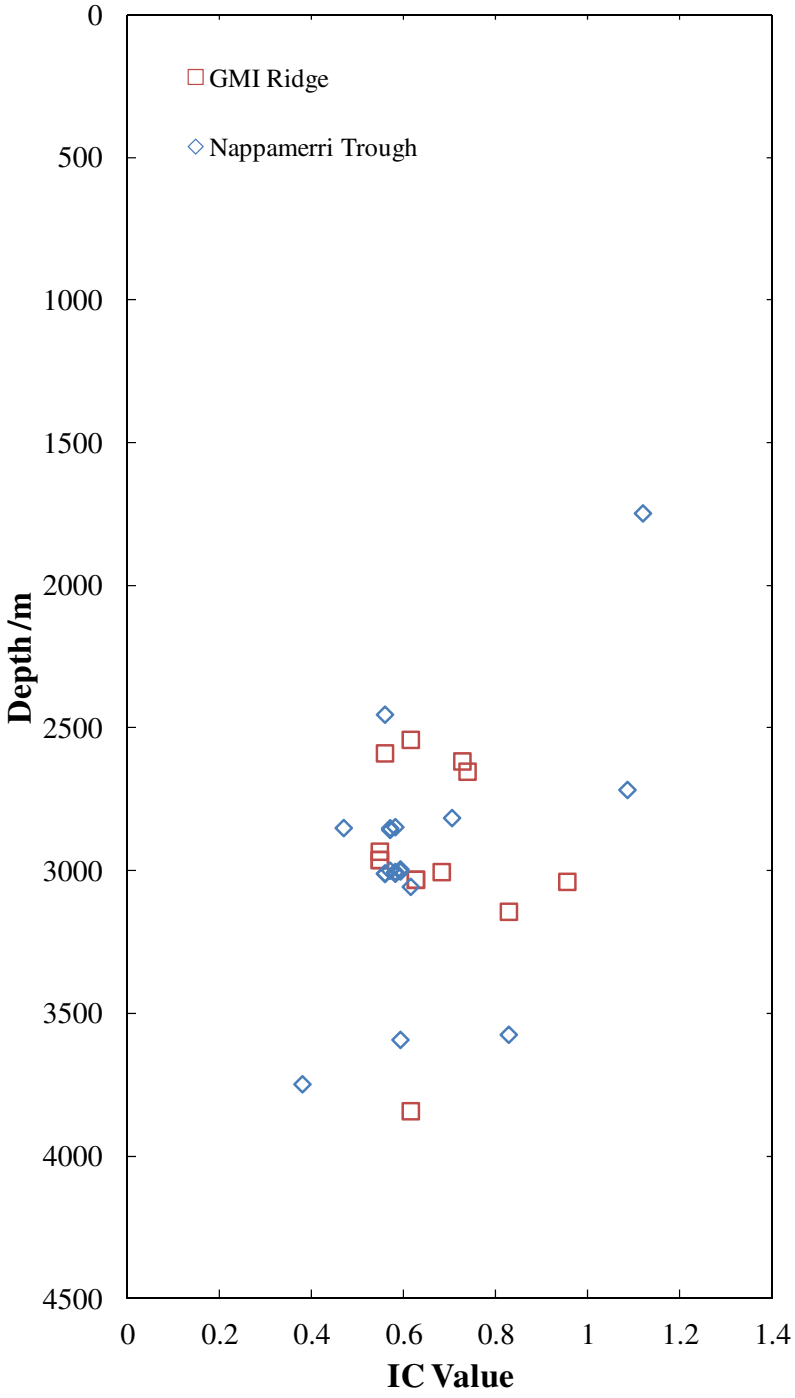

Figure 3

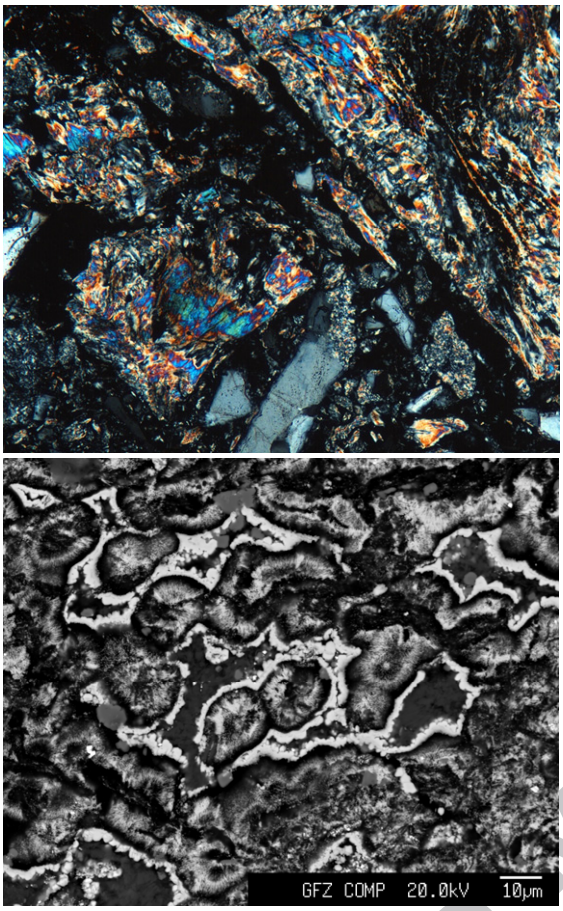

Figure 4

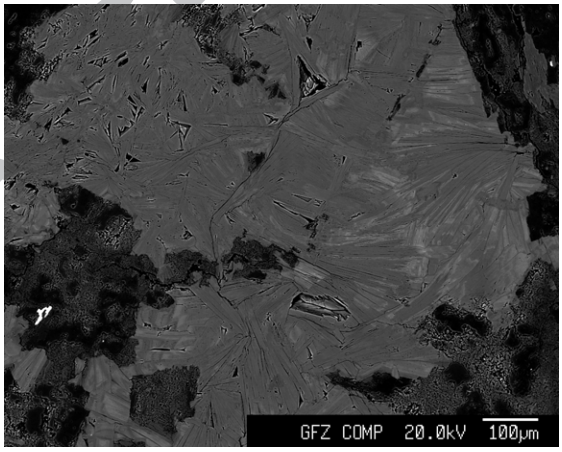

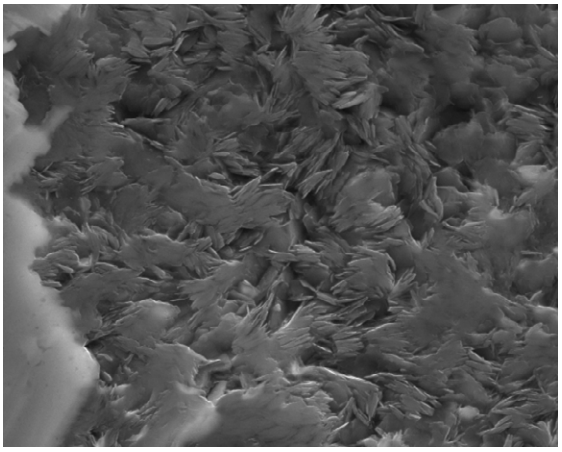

Figure 5

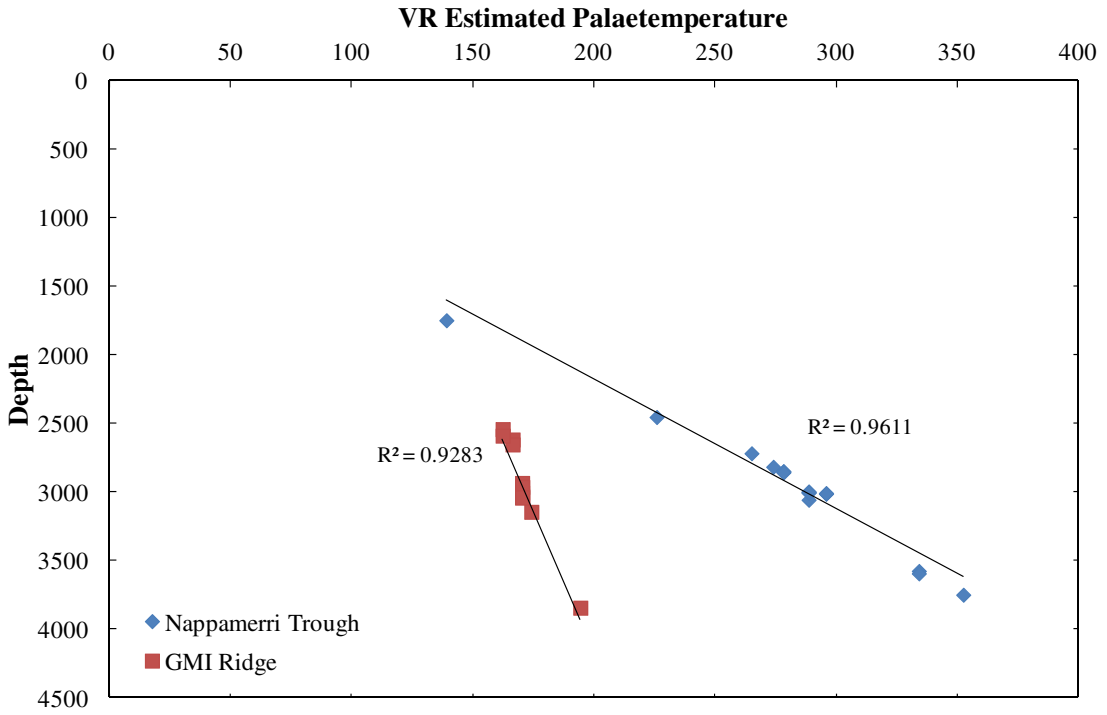

Figure 6

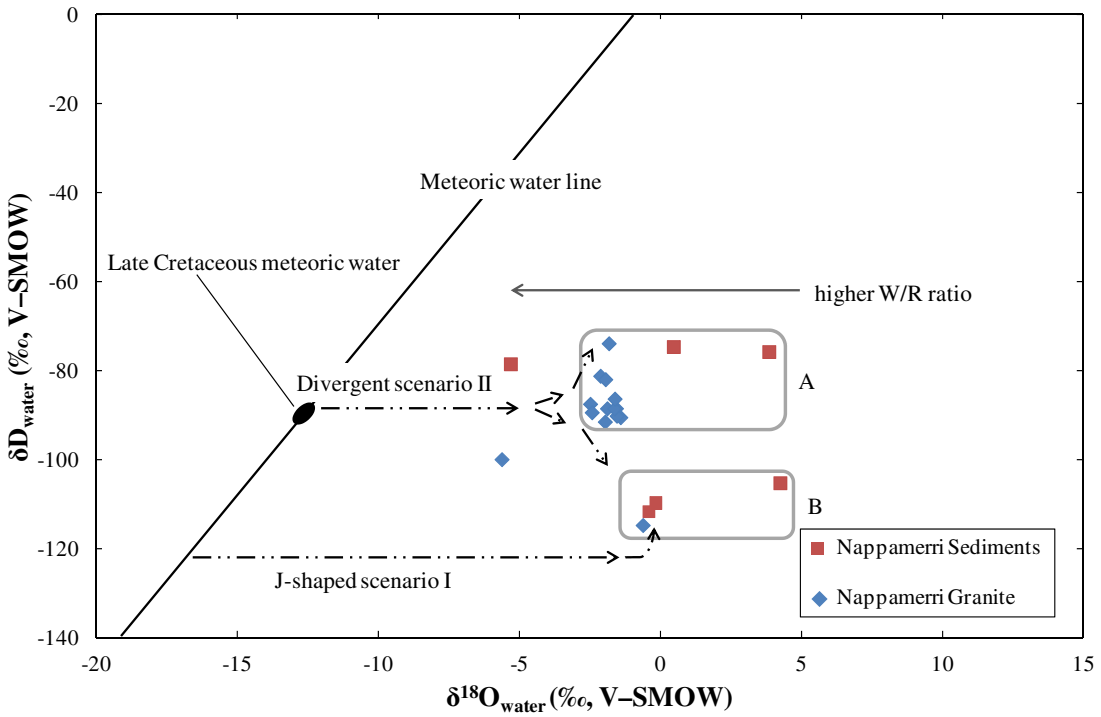

Figure 7

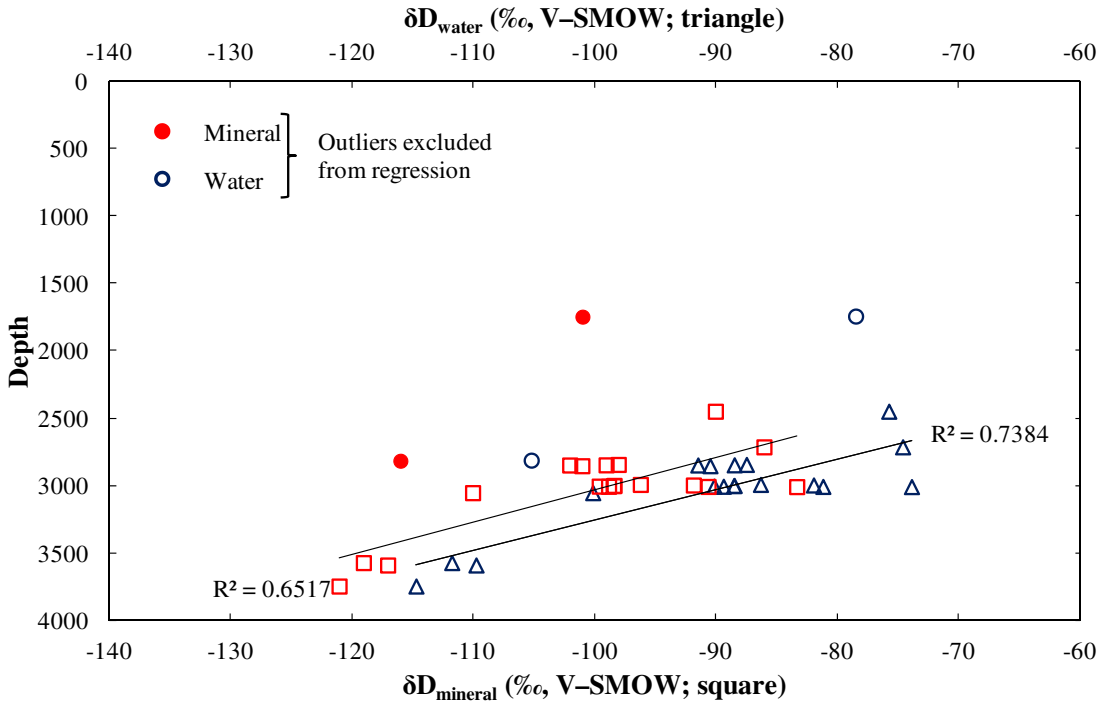

Figure 8

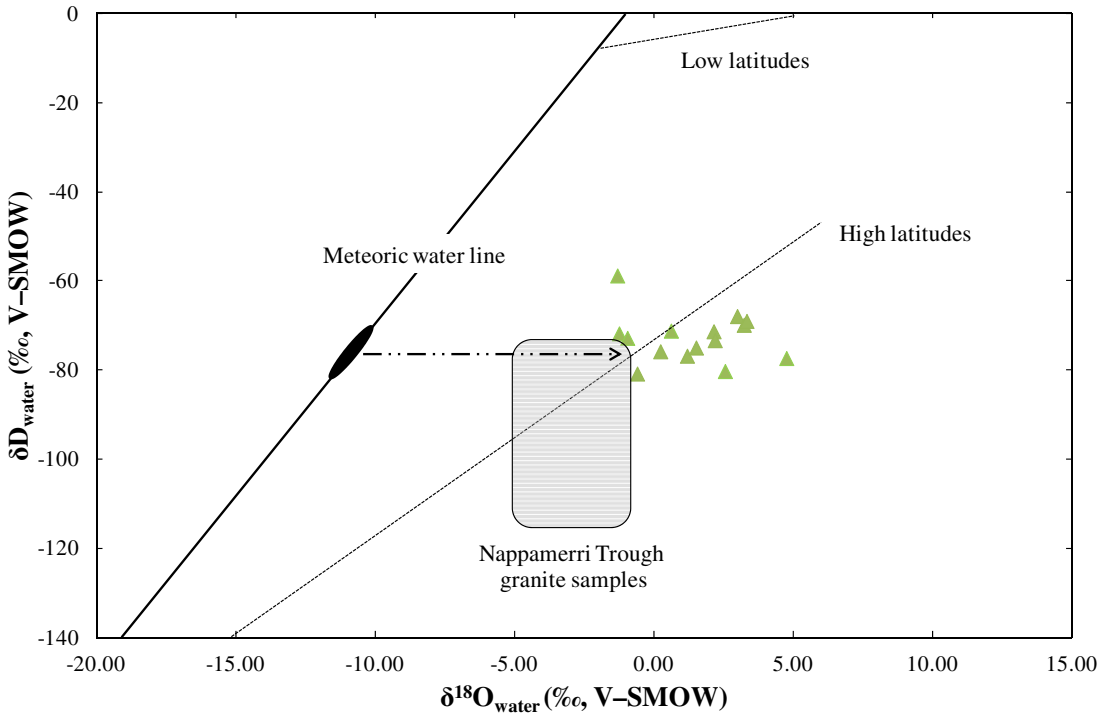

Figure 9

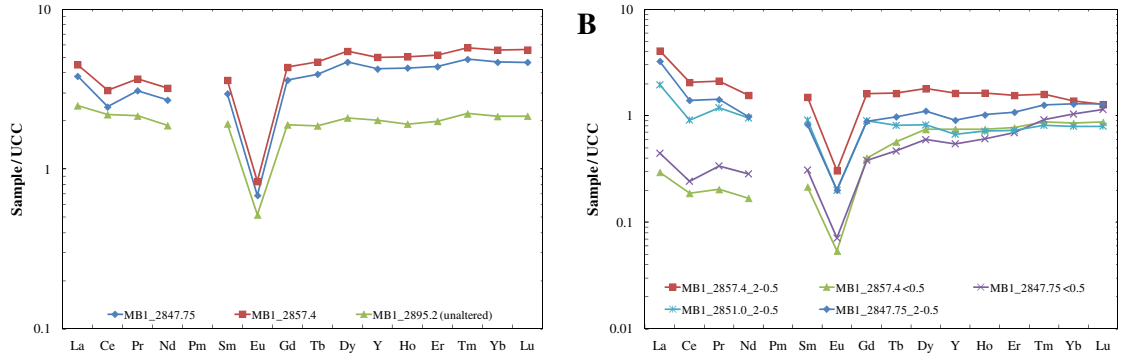

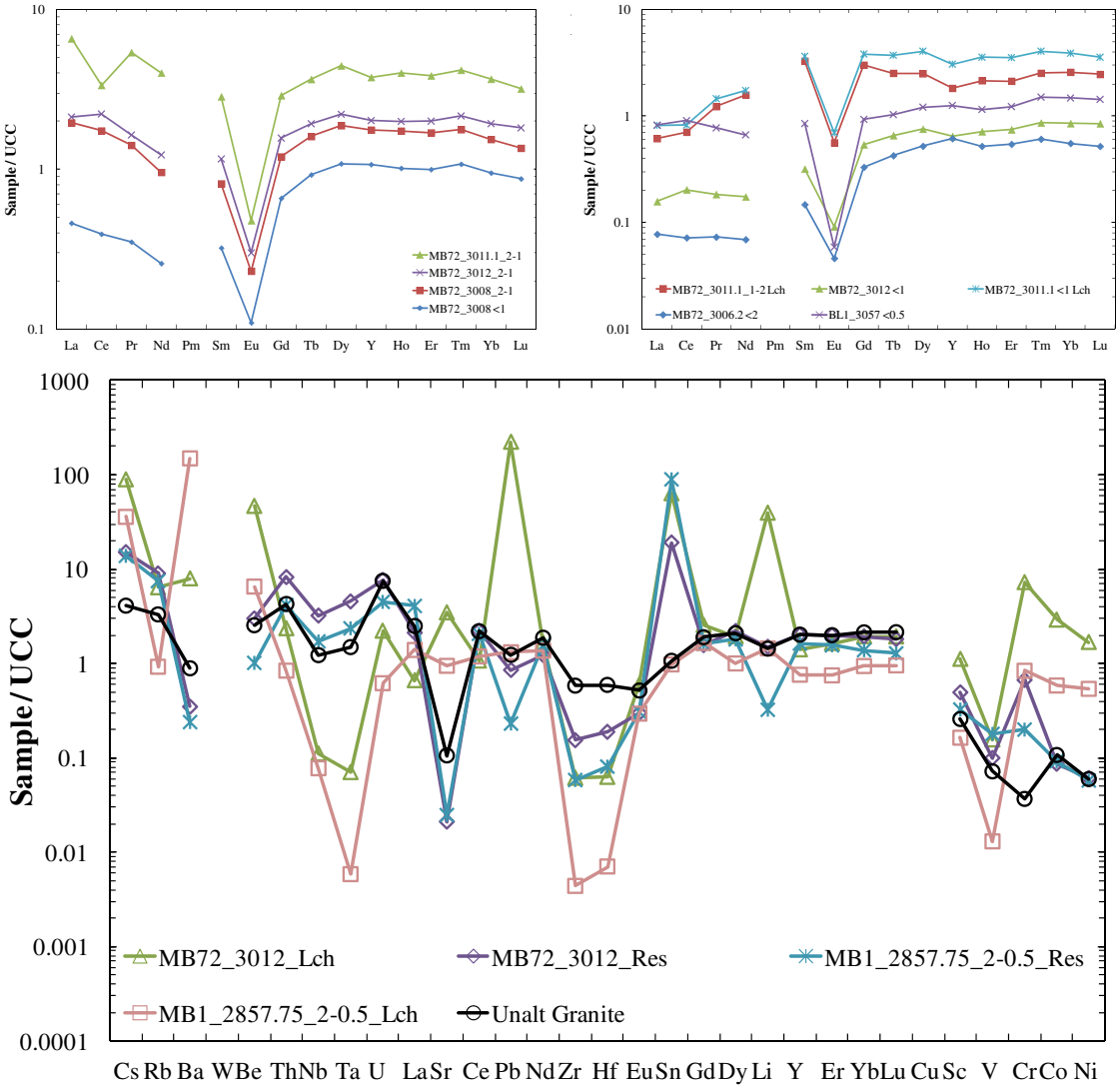

Figure 10

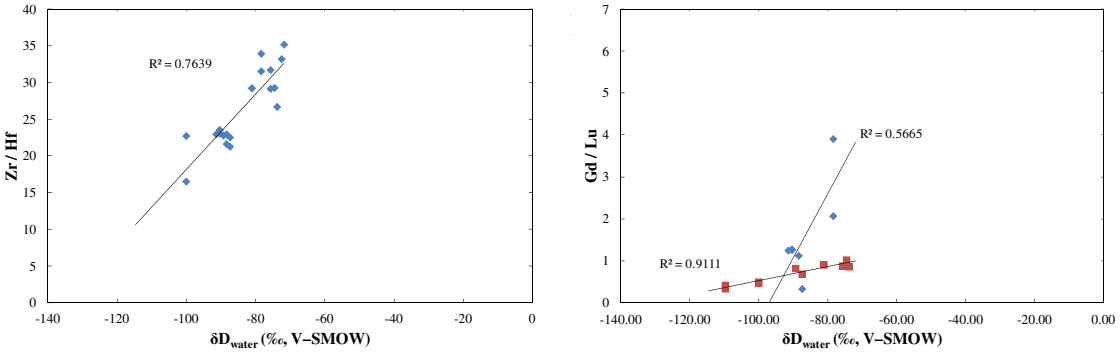

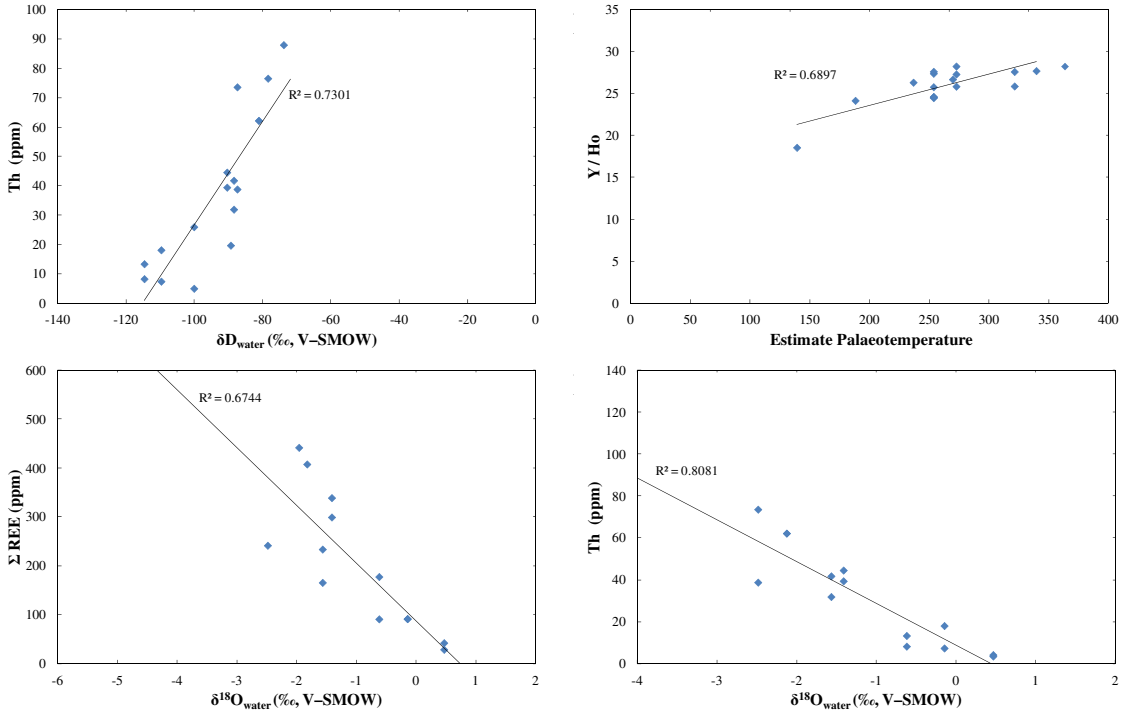

Figure 11

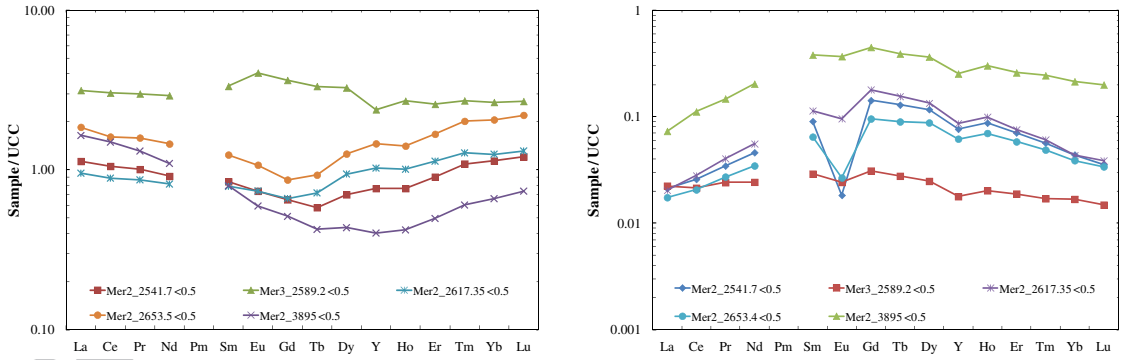

Figure 12